

SELECTION OF MICROMILLING CONDITIONS FOR IMPROVED
PRODUCTIVITY AND PART QUALITY

by
GÖZDE BULGURCU

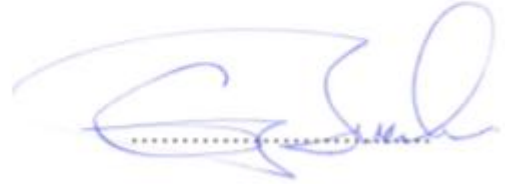
Submitted to the Graduate School of Engineering and Natural Sciences
in partial fulfilment of the requirements for the degree of
Master of Science

Sabancı University
February, 2017

SELECTION OF MICROMILLING CONDITIONS FOR
IMPROVED PRODUCTIVITY AND PART QUALITY

APPROVED BY:

Prof. Dr. Erhan Budak
(Thesis Supervisor)



Assoc. Prof. Umut Karagüzel



Assoc. Prof. Burç Mısırlıoğlu



DATE OF APPROVAL: 28.07.2017

© Gzde BULGURCU, 2017
All Rights Reserved

Annem'e

ve

Babam'a

SELECTION OF MICROMILLING CONDITIONS FOR IMPROVED PRODUCTIVITY AND PART QUALITY

GÖZDE BULGURCU

Industrial Engineering, MSc. Thesis, 2017

Thesis Supervisor: Prof. Dr. Erhan BUDAK

ABSTRACT

Micromilling process has a rising demand in recent years where the production industry is becoming more competitive with the advancing technology. In hi-tech industries such as aerospace, biomedical, electronics, the increasing demand for high precise micro products with complex geometries create necessity to improve micro machining processes for more accurate, repeatable, and efficient production.

Micro end milling process is relatively a new developing research area. It varies from conventional milling with its unique cutting dynamics due to the geometrical size reduction. In terms of the both micro tool and the workpiece, size reduction brings new difficulties to the process. The ratio of hone radius to uncut chip thickness creates a great difference between micro and conventional milling processes and precludes the application of conventional milling models to micromilling process. By the nature of the micromilling and its industries of usage, high accuracy and surface quality is expected in micro products. This makes the surface roughness and burr formation critical for micromilling process. On the other hand, since micro tools with very small radii are more fragile than conventional milling tools, workpiece-tool contact and cutting forces have also a remarkable

importance. Due to the same reason, tool costs and tool life are another significant point. All of these conditions make pre analysis and the parameter selection of micro end milling process essential for micromilling.

The main aim of this research is to determine micromilling parameters and conditions for improved productivity and part quality by considering multiple constraints and objectives at a time, unlike the previous studies on micro end milling process optimization which are limited and focus to optimize one objective at a time. The objectives in this study are the production time and production cost. Production time involves the actual cutting time, which involves the calculation of material removal rate (MRR), tool idling and changing time and time spent without any cutting. In production cost, tool costs, which is related with the tool life, machine idling costs, labour and overhead costs are included. Production time and cost are minimized respecting certain values of cutting forces, burr size and surface quality constraints. The effects of parameters; cutting speed, feed rate, and depth of cut on these objectives and constraints were investigated. For the first time, parameter selection in micro end milling process is done through multi-objective optimization using Particle Swarm Optimization method. Optimal process parameters are proposed for minimum process cost and minimum process time.

Keywords: Micro end milling, Multi-objective optimization, Parameter selection, Tool life, Production time, Production Cost, Surface roughness, Burr height, Cutting forces

ÖZET

Mikro frezeleme operasyonu, üretim endüstrisinin gelişen teknolojinin etkisiyle daha rekabetçi bir hale gelmesi ile son senelerde daha yüksek talep görmeye başlamıştır. Havacılık, biyomedikal, elektronik gibi ileri teknoloji endüstrilerinde, karmaşık geometriye ve yüksek hassasiyete sahip mikro parçacık ihtiyacının artması beraberinde mikro işleme operasyonlarının daha hassas, tekrarlanabilir ve verimli gerçekleştirilebilmesi gereksinimini getirmiştir.

Mikro frezeleme operasyonu yeni gelişmekte olan bir araştırma alanıdır. Mikro frezeleme operasyonu, takım ve iş parçasındaki boyut küçülmesinin sebep olduğu, kendine özgü kesme dinamiğiyle geleneksel frezeleme operasyonundan çok önemli farklılıklar taşımaktadır. Mikro frezeleme operasyonunun kullanım alanlarında, parçalarda yüksek hassasiyet ve yüzey kalitesi beklenmektedir. Bu nedenle, yüzey pürüzlülüğü ve çapak oluşumu mikro frezeleme için önemli kriterlerdir. Öte yandan, mikro frezeleme operasyonlarında kullanılan takımın çok küçük yarı çapa sahip olması ve dolayısıyla geleneksel freze takımlarından çok daha kırılgan olması, takım-ış parçası temasını ve kesme kuvvetlerini daha önemli bir hale getirmektedir. Aynı sebepten ötürü, takım maliyetleri ve takım ömrü önem kazanan noktalardır. Takım ucu radyüsünün kesilmemiş talaş kalınlığına olan oranı operasyon şartlarını oldukça değiştirmektedir ve bu durum geleneksel frezeleme operasyonu üzerinde yapılan çalışma ve modellemeleri mikro frezeleme operasyonuna uygulamayı imkansız kılmaktadır. Bu oran ve mikro boyutlar aynı zamanda çapak oluşumuna ve ısı üretimine ayrı bir önem kazandırmaktadır. Bu koşullar, mikro frezeleme operasyonlarında ön analizin ve parametre seçiminin önemini vurgulamaktadır.

Bu tez çalışmasının ana amacı, çok amaçlı eniyileme yöntemi kullanarak, mikro frezeleme operasyonunda parametre ve koşulların, üretim performansını ve parça kalitesini artırmaya yönelik belirlenmesidir. Daha önceki yapılan bir çok çalışma oldukça sınırlıdır ve tek seferde tek amaç hedeflenerek eniyileme yapılmıştır. Bu tez çalışmasında üretim süresi ve maliyeti minimize edilmeye çalışılmıştır. Üretim süresi, asıl kesme süresi, kesme yapılmayan süre, ve takımın boşa çalıştığı süreleri kapsamaktadır. Malzeme kaldırma hızı hesaplamaları, asıl kesme süresine dahil edilmiştir. Üretim maliyeti ise takım maliyeti, ve üretim süresine bağlı olarak işgücü maliyetlerini kapsamaktadır. Üretim maliyetinin önemli bir kısmını takım maliyetleri oluşturur, ki bu da

doğrudan takım ömrü ile alakalıdır. Yüzey pürüzlülüğü, çapak boyutları ve kesme kuvvetleri ise belirli değerlerin altında tutulmaya çalışılmıştır. Kesme hızı, ilerleme hızı, ve kesme derinliği değerlerinin etkileri araştırılmış ve bu değerler optimize edilmeye çalışılmıştır. İlk defa, mikro frezeleme operasyonu, Parçacık Sürü Optimizasyonu yöntemi ile çok kriterli eniyileme problem olarak modellenmiştir. En az maliyet ve en hızlı üretim göz önünde bulundurulacak şekilde parametre seçimi sunulmuştur.

Anahtar Kelimeler: Mikro-frezeleme, Çok kriterli eniyileme, Parametre seçimi, Üretim maliyeti, Üretim süresi, Takım ömrü, Yüzey pürüzlülüğü, Çapak yüksekliği, Kesme kuvvetleri

ACKNOWLEDGEMENTS

I would like to express my sincere appreciation to my thesis advisor Prof. Dr. Erhan Budak, for their patience, advice and continuous contributions to me and my study.

I would like to thank to my committee members; Assoc. Prof. Dr. Umut Karagüzel and Assoc. Prof. Dr. Burç Mısırlıođlu, for their time and comments.

I have to thank to Samet Bilgen, for being the best friend and love, for being the most supportive one, as always.

I also would like you thank to my fellow friends, Turgut Köksal Yalçın, Mehmet Albayrak, Hayri Bakkalođlu, Can Unutmazlar, Cihan Özener and Mert Kocaefe for both informative and amusing times spent together.

I would like to thank my brother, Berkehan, for his emotional support.

Lastly, I would like to thank my mom, Ayşen and my dad, Levent, for their eternal support and sacrifice.

TABLE OF CONTENTS

1. INTRODUCTION.....	1
1.1 OVERVIEW	1
1.2 THESIS OUTLINE	3
2. LITERATURE SURVEY.....	5
2.1 OVERVIEW	5
2.2 TOOL LIFE	5
2.3 MATERIAL REMOVAL RATE	7
2.4 SURFACE ROUGHNESS	7
2.5 BURR FORMATION	8
2.6 CUTTING FORCES	11
2.7 TOOLING PERFORMANCE: MATERIAL, COATING, AND GEOMETRY DESIGN.....	13
2.8 PROCESS PARAMETERS	16
2.9 MULTIPLE OBJECTIVE OPTIMIZATION METHODS.....	18
2.10 OBJECTIVE AND MOTIVATION	22
3. UNIQUE MECHANISMS OF MICROMILLING.....	23
3.1 FUNDAMENTALS	23
3.2 MINIMUM CHIP THICKNESS AND PLOUGHING EFFECT.....	24
3.3 CHIP REMOVAL PROCESS AND CONSEQUENCES	26
4. OPTIMIZATION OF MICROMILLING.....	28
4.1 MULTIPLE OBJECTIVE PARTICLE SWARM OPTIMIZATION (MOPSO)	28
4.2 OBJECTIVE FUNCTIONS.....	31
4.2.1 <i>Production Time</i>	31
4.2.2 <i>Production Cost</i>	33
4.3 CONSTRAINTS	34
4.3.1 <i>Surface Roughness</i>	34
4.3.2 <i>Burr Height</i>	38
4.3.3 <i>Cutting Forces</i>	41
4.4 OPTIMIZATION OF MICROMILLING PROCESS	51
4.5 SUMMARY	54
5. APPLICATIONS AND CASE STUDIES.....	55
5.1 VERIFICATION TEST SETUP.....	55

5.2	RESULTS AND DISCUSSIONS	59
5.2.1	<i>Production Time</i>	59
5.2.2	<i>Production Cost</i>	61
5.2.3	<i>Surface Roughness</i>	62
5.2.4	<i>Burr Formation</i>	64
5.2.5	<i>Cutting Forces</i>	66
5.2.5	<i>Summary</i>	67
6.	CONCLUSION	69
7.	REFERENCES	71

LIST OF FIGURES

Figure 2.1 - Schematics of poisson burr, tear burr and roll-over burr [22].....	9
Figure 2.2 - Types of burrs in end milling [5].....	10
Figure 2.3 - Slip-line Field Theory [41].....	12
Figure 2.4 - (a) Two-flute end mills, (b) Triangle type end mills with a straight body, (c) D-type end mills with a straight body, (d) triangle type end mills with a tapered body, and (e) D-type end mills with a tapered body	15
Figure 2.5 - (a) Dominated solution in two objective space; (b) The Pareto front of a solution set in two objective space [65].....	19
Figure 3.1 - Nanofocus image from a flute of a 2mm micro end mill	24
Figure 3.2 – (a) Macro-milling; (b)Micromilling [1].....	25
Figure 4.1 - Cutting tool profile in micromilling [23].....	34
Figure 4.2 - Material removal process in trochoidal tool path	35
Figure 4.3 – Minimum chip thickness and plastically deformed area	36
Figure 4.4 - Case 1: $f_t < t_c$	37
Figure 4.5 – Case 2: $f_t > t_c$	38
Figure 4.6 – (a) Exit geometry in micromilling; (b) Geometry of burr formation [28]	39
Figure 4.7 - Primary, secondary and tertiary deformation zones	42
Figure 4.8 - Regions on the rake face of the tool	43
Figure 4.9 – Third deformation zone regions and ploughing depth.....	47
Figure 4.10 - MOPSO parameters.....	51
Figure 4.11 - (a) Max. iteration =100; (b) Max. iteration = 150; (c) Max. iteration = 200.....	52
Figure 4.12 - Pseudo-code of MOPSO.....	53
Figure 4.13 - Pareto curve generated by MATLAB code	54
Figure 5.1 – (a) Tool and Workpiece Setup, (b) Slot Milling Operation.....	56
Figure 5.2 – (a) KERN Evo Ultra Precision Machining Centre; (b) Kistler Type 9256C; (c) Nanofocus μ surf Explorer	57
Figure 5.3 - Hone Radius Measurement under Nanofocus μ surf.....	57
Figure 5.4 -- Measured production time vs calculated production time	59
Figure 5.5 - Example of Pareto curve generated by MATLAB code	60

Figure 5.6 - Production time with recommended cutting parameters vs optimized cutting parameters	60
Figure 5.7 – Sample measurements of final tool hone radii; (a) with recommended parameters; (b) with optimized parameters	61
Figure 5.8 – Tool wear with recommended cutting parameters vs optimized cutting parameters	62
Figure 5.9 - Measured surface roughness vs calculated surface roughness	62
Figure 5.10 - Nanofocus image and measurement table of a chatter vibration detected	63
Figure 5.11 - An example measurement of surface roughness from tests with recommended cutting parameters	63
Figure 5.12 - - An example measurement of surface roughness from tests with optimized cutting parameters	63
Figure 5.13 - Surface roughness with recommended cutting parameters vs optimized cutting parameters	64
Figure 5.14 - Burr size measurement	65
Figure 5.15 - Burr images from slots with recommended cutting parameters	65
Figure 5.16 - Burr images from slots with optimized cutting parameters.....	65
Figure 5.17 - Measured Feed Force vs Calculated Feed Force	66
Figure 5.18 - Measured Tangential Force vs Calculated Tangential Force	67
Figure 5.19 – Cutting forces with recommended cutting parameters vs optimized cutting parameters	67

LIST OF TABLES

Table 2.1- Tool material performances [48]	13
Table 2.2 - Tool materials and their applications on workpiece materials [48].....	13
Table 5.1 –First set of tests with recommended cutting parameters	55
Table 5.2 – Second set of tests with code generated cutting parameters	56
Table 5.3 - Results from recommended cutting parameters.....	58
Table 5.4 - Result from optimized parameters achieved by experimental measurement and model	58
Table 5.5 - Johnson's Cook parameters for Ti-6Al-4V	66

NOMENCLATURE

C_{total}	Total Production Cost
d	Depth of Cut
f	Feed Rate (mm/min)
f_t	Feed per Tooth (mm/tooth)
F_f	Feed Force
F_t	Tangential Force
h	Chip Thickness
i	Helix Angle
n	Spindle Speed
R	Cutting Tool Radius
r_c	Hone Radius (Cutting Edge Radius)
R_a	Surface Roughness Average
R_t	Maximum Height of the Surface Profile
t_c	Minimum Chip Thickness
t_0	Uncut Chip Thickness
T_{Life}	Tool Life
T_{total}	Total Production Time
V_C	Cutting Speed (m/min)
z	Number of Teeth
β	Shear Angle
β_o	Initial Shear Angle
\emptyset	Instantaneous Immersion Angle
θ	Tool Rotation Angle

1. INTRODUCTION

1.1 Overview

With the rapid technological advancements in recent years, mechanical components and parts are becoming tinier. Especially in aerospace, biomedical, electronics and optics industries, for the production of micro dies and moulds, high precision is required in miniature and complex structures.

Many different micro machining techniques can be used to respond dimensional accuracy and surface quality needs such as additive techniques, lithographic processes, laser, ultrasonic etc. In some cases, those micro machining processes cannot be used due to the workpiece material, operational difficulties and expensive or time consuming solutions. Micromilling is one of the micro manufacturing techniques which is widely preferred when process flexibility and material variety is needed. It is the right solution to machine high strength workpiece materials with complex details. In order to maintain high precision requirements with the high process performance, process modelling, cutting tool and parameter selection are the key considerations.

Popular usage of micro end milling in recent years accelerated the process development for improved process capabilities. A research on micromilling shows that the process fundamentals are different from conventional milling in terms of dynamics, kinematics, chip formation, heat generation and tool-workpiece contact [1]. The developments on micromilling are mainly concentrated on reducing the production cost and reducing the production time while obtaining a high surface quality.

One of the important issues in micromilling is tool wear and tool life. Tools with diameters smaller than 1 mm are weaker and more expensive compared to conventional milling tools. In addition to wear, they can easily be damaged due to micro vibrations, excessive heat and rubbing [1]. Parameter selection for maximizing the tool life can considerably reduce the production cost.

Material removal rate is remarkably low in micromilling since uncut chip thickness is less than few microns. In order to shorten production time, MRR is kept at maximum values without sacrificing

process quality. By the fine selection of process parameters, the uncut chip thickness should be kept at maximum to maximize the material removal rate [2].

Excessive cutting forces may lead to early tool breakage and poor part quality. In micromilling, hone radius has a remarkable effect on cutting forces [3]. The effect of hone radius can mostly be neglected in conventional milling, since the hone radius is very small compared to other tool dimensions and parameters. Since conventional tools can be considered as sharp. However, hone radius has a considerable size in micromilling relative to the other cutting dimensions and the cutting forces are directly affected by the hone radius [1]. In order to avoid excessive cutting forces, hone radius selection is very important [4].

Other important criteria in selection of milling conditions are the burr formation and surface quality. Burr formation is hard to be avoided; however, it can be minimized under acceptable values. Excessive burr sizes cause poor part precision and high heat generation which may lead to early tool breakage [5]. On the other hand, surface roughness should also be controlled to maintain geometrical accuracy.

From the manufacturer's perspective, these conditions should be considered simultaneously; conditions optimizing one objective does not make sense commercially. Minimizing surface roughness may degrade production time or tool life, or vice versa. Therefore, product quality and process performances should be maximized together in micromilling operations. Conditions should be determined to maintain a better tool life, better product quality while minimizing production cost and time.

As mentioned, problems in micromilling can be summarized as; premature tool breakages, high accuracy demand with low surface roughness and burr sizes, while maintaining low production cost and production time. Such problems as micromilling which include multiple conflicting objectives and parameters can be solved by different multi-optimization techniques. Unlike single optimization problems, for multi-objective problems (MOOPs), a set of feasible solutions are found in which all the solutions are non-dominating each other. Each of these solutions are a better respond to a different objective function. Considering the weight of the selected objective function

importance, preferred solution can be chosen among the list of the solutions by a decision maker (DM).

In this research, the aim is to optimize micromilling process for a minimum production time and production cost considering the process limitations. Tool life and material removal rate (MRR) will be included in the calculations of these objective functions. Surface roughness, burr height and cutting forces are to be kept under acceptable values during process optimization for a developed process performance and part quality.

MATLAB code is going to be developed outputting the optimized values for the cutting speed, feed rate, and depth of cut aiming minimized production time and cost. The algorithm is a particle swarm optimization algorithm, which depends on the idea of moving particles towards the best positioned particles. A Pareto curve is created representing particles giving the minimum production cost and production time.

1.2 Thesis Outline

The main objective of this thesis is to obtain process parameters for an optimized micromilling operation of a product considering production efficiency and part quality. MATLAB code has been developed for this multi objective optimization problem where experimental applications have been completed in order to support code outcomes.

In Chapter 2, detailed literature survey about micro end milling process, multi objective problem solution methods and formulations of objective functions and constraints that are presented.

Chapter 3 presents more unique mechanisms of micromilling process in details. In this chapter, size effect, minimum chip thickness, chip removal process and effects of process parameters on process outcomes are evaluated in order to shed a light for further formulations which are going to be used in formulations for problem solution.

Chapter 4 will be the main chapter of the thesis in which the selected method for multi objective optimization problem is investigated. The objective functions and constraints will be explained in

details and formulations will be presented. In the last section of Chapter 4, MATLAB code algorithm will be explained and some parts of the code will be provided.

Experimental applications and case studies will be presented in Chapter 5. Results obtained by the algorithm will be compared with results from standard cutting parameters. The comparisons will be made in terms of production cost and time, as well as surface roughness, burr formation and cutting forces. Predicted results from the code will also be compared to experimental results achieved using the Pareto solutions.

In Chapter 6, summary, results and discussions will be given. Thesis conclusion and potential future work will be presented.

2. LITERATURE SURVEY

2.1 Overview

Micromilling is an emerging manufacturing field where high precision production is required. Findings regarding conventional milling cannot be applied to micromilling since micromilling gives different outcomes than expected. Researchers are trying to highlight how micromilling kinematics, dynamics and thermal aspects are affected by the size reduction. The purpose of this thesis is to optimize tool geometry and process parameters by taking multiple objectives into consideration. The optimization procedure considers tool life, MRR, surface roughness, burr height and cutting forces which are the main elements of micromilling, affecting efficiency and cost. The parameters which are going to be investigated are the most effective parameters on these objectives and constraints [6] [7], which are feed rate, uncut chip thickness and cutting speed. Micro end mill tool will also be investigated for optimal geometry. In this chapter, previous research studies that are conducted on related subjects will be presented.

2.2 Tool Life

Tool life has been a popular research area in micromilling since tool breakage is a frequently encountered problem when using tools in small diameters. Tool wear in micromilling is very hard to notice by process monitoring. Tool can break suddenly or product quality can be poor at the end because of the unnoticed tool wear. That is why tool wear is an important research area in micromilling to increase process quality. It is observed by Rahman et al. [8] that high cutting temperatures cause rapid tool wear and the cutting forces should be kept minimum. In another article, Tansel et al. [9] stated that high feed rates causes abrasive wear which results in increased cutting edge radius and ploughing force. Martin et al. [10] concluded that the while machining aluminium, higher cutting speeds increases tool life.

Recent studies on tool life mostly depend on experimental curve fitting implications to a very earlier and well-known modelling of Taylor [11]. In later studies, researchers generally add unknown exponents with specific parameters and implement experimental data to Taylor's formulation. In one of those researches, Wu [12] estimated tool life by surface response

methodology and took feed rate, f and depth of cut, d into consideration. Later on, Kuljanic and Solaja [13] stated that the depth of cut is not too important to consider in such equation, depending on the fact that the exponent of depth of cut is found out to be negative in many researches.

There are also other conditions and parameters which should be considered to maximize tool life. Especially for the hard workpiece materials, tool life is limited due to high wear rate. Kajaria [14] worked on the tool coatings and lubrication conditions to increase tool life in micromilling. He investigated the tungsten carbide end mills coated with TiN, Ti-AlN, Ti-CN under dry, mist (2210 EP and blasercut mist) and wet (blasercut flood) conditions. Aramcharoen et al. [1] stated that the cutting edge of the tungsten carbide micro end mills is generally broken when the coating layer is peeled off. Among the coating materials, TiN is found to be more protective compared to TiAlN, TiCN, CrN and CrTiAlN.

Other approaches include investigations of cutting parameters which increase tool life. Rahman et al. [8] suggested that the increase in depth of cut increases the tool life while increase in cutting speed decreases the tool life. His suggestion is an expected one since the high cutting speeds causes more heat generations; similarly Liu [15] stated that the high cutting temperature speeds up the tool wear rate.

Guimaraes et al. [16] used data acquisition techniques and demonstrated that there is a high correlation between the cutting forces and tool wear. Their results agreed with the Taylor's tool life equation [11]. Twardowski et al. [17] investigated tool wear and tool life of coated carbide and cubic boron nitride tools. They used different tool geometries and found out that after a critical cutting speed, tool life has a sudden decrease. The decrease is at higher cutting speed when using ball end mill cutters than toroidal milling cutters. They also experienced that boron nitride edges can resist to higher cutting speeds.

It is shown that the studies on tool life have a wide range of topics; from geometrical analysis to coatings etc. Cutting parameter analysis is a common and practical method for maximizing tool life in many applications.

2.3 Material Removal Rate

Material removal rate (MRR) is an important performance parameter in micromilling which affects process cost and production rate. In roughing operations, MRR has the primary importance to increase process performance.

One of the reasons to choose micromilling over other micro machining techniques is that it has relatively high MRR. However, due to the micromilling process nature, there are many limitations for obtaining higher MRRs, such as small uncut chip thickness due to weak cutting edges and tools. MRR can be considerably increased by adjusting the process parameters.

The researches on MRR in micromilling generally focuses on optimization of cutting parameters to increase MRR. Periyanan et al. [18] used Taguchi method to optimize cutting parameters to achieve high MRR considering the spindle speed, feed rate and depth of cut. They found out that the optimal parameter combination to maximize MRR is medium cutting speed, high feed rate and high depth of cut.

One of the other approaches to maximize MRR is by federate scheduling. Merdol and Altintas [19] maximized MRR by calculating maximum allowed federate and spindle speed for each cutter locations for an oblique cutting operation.

Tool life and process performance criteria, such as surface roughness and chatter, limit MRR. However, increasing MRR while staying under the limitations is possible through optimizing process parameters.

2.4 Surface Roughness

Especially in finishing operations, surface roughness carries primary importance for increased part quality. For micromilling, high precision products necessitate good surface finish. The research on surface roughness is generally on studies with surface roughness modelling or parameter selection. Studies which aim to optimize process parameters to decrease surface roughness shows that unlike conventional milling, decreasing the feed rate, and thus chip thickness, may cause ploughing which

would result in increasing the cutting forces and the surface roughness in micromilling [20] [21] [22].

Many researchers studied surface roughness because of its high importance in micromilling. Different surface roughness models exist, considering the cutting duration, chip formation dynamics, tool and process geometries, and the dynamics special to micromilling such as minimum chip thickness and ploughing effect. In all modelling attempts, it is observed that the most affecting parameters are the minimum chip thickness, ploughing mechanisms and the feedrate among the cutting parameters [23] [24]. In another research, it is claimed that the increase in the cutting edge radius also increases the surface roughness and the critical chip thickness, which is the minimum chip thickness value that the tool is able to remove which is usually around 20-40% of cutting edge radius [25]. Another research about micromilling of aluminium, supports the previous study by claiming the ratio of minimum chip thickness-to-cutting edge radius as 30% [26].

Surface roughness is evaluated from different aspects in different studies. Some studies try to optimize average roughness (R_a) which is the arithmetic average of the absolute values of the profile heights through the evaluation line, whereas some studies consider the average maximum length of the profile (R_z), and some studies try to minimize maximum height of the profile, (R_t). In his thesis, Hatipoglu [27] investigated surface formation and affecting parameters to model surface roughness. After his experimental studies, he found out that the depth of cut increases cutting temperature and chip formation. As the feed rate and cutting speed increases, burr formation is reduced. Deriving from process geometry, he has modelled and verified the surface roughness which will be given in details in Chapter 4.

2.5 Burr Formation

Burr is initially defined by Ko and Dornfeld [28] as the workpiece extension on its edge or surface which is not a desired geometry. Burr formation is more important in micromilling since it is more essential to achieve product precision and accuracy in miniature parts. The dimensional accuracy and surface quality highly demand on burr formation. It may be impossible to achieve totally burr-free parts in many applications, but burr sizes can be reduced under acceptable limits.

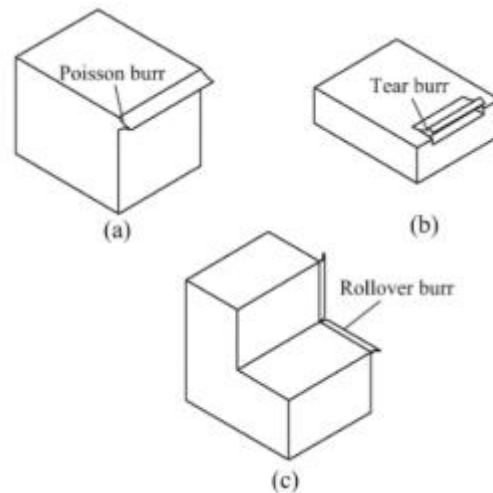


Figure 2.1 - Schematics of poisson burr, tear burr and roll-over burr [22]

Researches classify burrs in terms of their cause, location, shape and formation mechanism. There are three main types of burr formation, as shown in Figure 2.1, caused by different reasons such as bulging of the material at the sides when compressed (poisson burr), tearing of the material (tear burr) and bended chip rather than sheared (roll-over burr) which is the most common of all [29]. In terms of locations, burrs are classified according to their locations (see Figure 2.2) where exit burr is the most common.

The measurement of the burr sizes also vary from study to study. Some studies measure burr heights, some measure burr width or the thickness, which are the most common detection methods. There are also studies measuring burrs with their volume or even the hardness. Stylus method, metallographic profile, optical microscope and SEM are some of the devices used to measure burr sizes.

Burr formation depends on the workpiece material, tool geometry and process parameters. There are different approaches to the complex mechanisms of burr formation and minimization methods in literature either by controlling or preventing, or removing as a separate process. Chu and Dornfeld [30], suggest different ways to minimize burrs for various workpiece materials. Gillespie and Blotter [31] examine the effect of process parameters on burr formation and formation mechanisms of different burr types. To control burr formation, Kou et al. [29] employed supporting material on top of the workpiece and increased workpiece rigidity. Komatsu et al [32] examined the grain size effect on burr formation and applied micromilling tests on stainless steel. They argued

that it is possible to minimize burr by decreasing grain sizes. Saptaji et al. [33] investigated the effects of side edge angle and effective rake angle on top burr formation. There are many other studies work on the process parameter effects on burr formation [34] [6]. Chen et al. [35] observed burr formation in slot milling process while using titanium alloy as the workpiece material and modelled burr formation mechanism. Schueler et al. [36] also used titanium alloy and examined micro end milling operations.

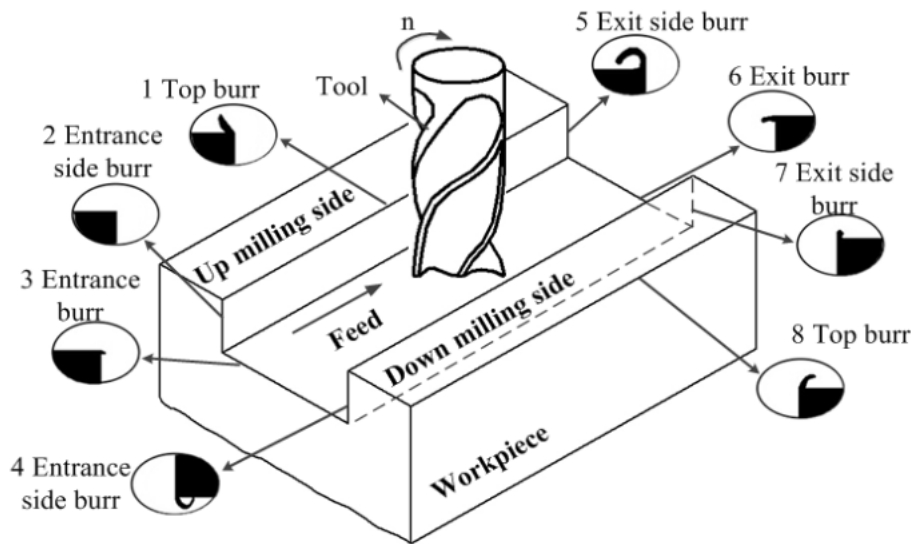


Figure 2.2 - Types of burrs in end milling [5]

An extensive research on burr formation in micromilling [5] concludes that the burr formation is the result of three mechanisms; lateral deformation of the material, bending and tearing of the chip. It is observed that the depth of cut and the tool diameter are the main parameters affecting burr height and thickness, but ANOVA analysis shows that number of flutes, feed rate and their interaction determines the 95% of burr height and burr width [5]. For the minimization of the burr size, high feed rates, tool diameter and number of flutes should be selected. From process geometry, they derived a model predicting burr height with a low accuracy within 0.65-25% [5].

Besides the surface roughness, minimum chip thickness and the ploughing effect also increase the burr formation. As the federate increases, it is observed that the burr formation decreases [22]. Weinert et al. stated that the ratio of minimum chip thickness to tool cutting edge radius increases, burr formation also increases [37].

The effect of machining strategies on burr formation was investigated by Cardoso and Davim [38] who tested constant overlap spiral, parallel spiral and parallel zigzag techniques. The best burr height and surface roughness performances are achieved with constant spiral technique.

2.6 Cutting Forces

In micromilling, the control of cutting forces is very important due to flexible and weak cutting tool which may easily break. Force control can also provide a better tool life and good surface finish [27]. Micro tools are more prone to be affected by cutting temperatures and wear. It is observed by Rahman et al. [8] that high cutting temperatures speed up the tool wear rate and the cutting forces should be kept minimum. High cutting temperatures and a worn tool distorts the surface quality. Therefore, cutting forces need to be kept under critical values in micromilling for better process performances.

Due to the substantial size reduction from macro milling to micromilling, the process mechanisms totally differ from each other. The uniqueness of micromilling creates necessity to the unique mechanism modelling for micromilling. There are different approaches to model micromilling forces in the literature. Due to the size reduction effect, tool hone radius gains importance and it cannot be neglected as in macro-milling. It is proven that the hone radius has a great effect on cutting forces in micromilling [21]. Kim and Kim [39] modelled the cutting forces with considering the hone radius and ploughing mechanism. Bissacco et al. [40] also developed a cutting force model by calculating force components acting on the finite number of elements of the tool.

There are other approaches such as dividing the workpiece material into regions according to the type of the material deformation mechanisms. These regions are named primary, secondary and third deformation zones [41] as in Figure 2.3. This theory is called slip-line field theory. For rounded edge cutting tools, Fang [42] developed another cutting force model by using the slip-line field theory. Altintas et al. [43] developed an analytical prediction modelling. They also used slip-line theory for the prediction of material and friction effect on chip formation.

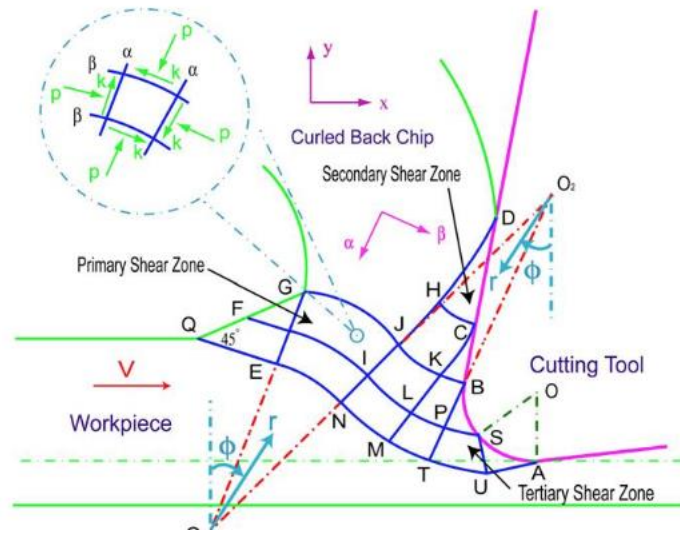


Figure 2.3 - Slip-line Field Theory [41]

There also mechanistic approaches which predicts cutting forces in micro end milling considering size effect, minimum chip thickness and ploughing mechanism [44] [45] [46] . For the investigation of the ploughing mechanism, they separated the cutting mechanisms as shearing dominant and ploughing dominant which changes with the varying chip thickness due to the trochoidal path of the tool.

Another modeling approach is the finite element analysis (FEM). Afazov et al. [47] used FEM analysis for micro end milling by using ABAQUS/Explicit. By using FEM approach, he included the material behaviour in his modelling.

Recently in his thesis, Hayri [3] developed a thermo-mechanical model which predicts cutting forces in micromilling by considering primary, secondary and third deformation zones separately due to unique deformation mechanisms taking place. When we consider the newly formed workpiece surface, cutting force is still observed even though shearing does not take place. This force is due to the continuous tool-workpiece contact in third deformation zone and the ploughing mechanism. In another work [48], they investigated the stagnation point, which separated the newly formed surface and chip formation. They stated that under stagnation point, peak in cutting force measurements are due to ploughing mechanism. Ploughing force has a high contribution to the total cutting forces.

2.7 Tooling Performance: Material, Coating, and Geometry Design

Small tool size may lead to sudden tool breakage in micromilling. Studies on tool selection includes tool geometry design and application of coatings. Tools in micromilling should be chemically stable under high temperatures. Micro tools are generally made up of high speed steels (HSS), carbide, ceramics, cubic boron nitride (CBN) or diamond (PCD). The performance of micro tool materials and their usage on different workpiece materials are listed by Childs [48] as in **Error! Reference source not found.** and Table 2.2. From the tables, the tool materials can be listed from the worse to the best as; HSS, carbide, ceramics, CBN and diamond. Of course, tool cost increases with the same order as well.

Table 2.1- Tool material performances [48]

	Hot hardness	Toughness	Wear resistance	Thermal shock resistance	Cutting speed	Surface finish	Material costs
High speed steel	Low	High	Low	High	Low	Low	Low
Carbide	↓	↑	↓	↑	↓	↓	↓
Ceramics	↓	↑	↓	↑	↓	↓	↓
CBN	↓	↑	↓	↑	↓	↓	↓
Diamond	High	Low	High	Low	High	High	High

Table 2.2 - Tool materials and their applications on workpiece materials [48]

	Soft non-ferrous	Cast iron	Carbon and low alloy steels	Hardened steels	Nickel-based alloys	Titanium alloys
High speed steel	√	×	O	×	×	×
Carbide	√	√	√	O	√	O
Ceramics	×	√	√	O	√	×
CBN	×	O	×	√	O	O
Diamond	√	×	×	×	×	√

(√: Good, O: Suitable, ×: to be avoided)

The hardness of the tool is not related with the tool wear resistance [49]. For instance, with tungsten carbide tools, generally high wear rate is observed. Coatings are applied on tools for more wear resistance and they may also provide lower friction between the tool and the workpiece. Aramcharoen et al. [1] investigated the effect of different coatings on tool wear and surface finish. They found out that TiN coating provides the longest tool life and the best surface quality among CrN, TiCN, TiAlN and CrTiAlN.

Sooraj and Mathew [7] used Taguchi's orthogonal array L18 to improve surface quality and top-burr width. They investigated the effects of tool type, cutting speed, feed per tooth and the axial depth of cut. Their result showed that top burr is higher in up milling operation and TiN coating created more top burr than an uncoated tool. However, tool with the TiN coating improves the surface quality. They saw that the increasing spindle speed and the feed per tooth caused more top burrs. Decreasing axial depth of cut also increased burr formation and it has more dominant effect on burr formation than other cutting parameters. On the other hand, increasing the spindle speed improved the surface finish, while decreasing the feed rate improved the surface finish.

With the right selection of tool geometry, tool stiffness can be increased further. By Finite Element Analysis, Li [50] claimed that the negative rake angle, and low helix and relief angle can lower down the maximum stress on the tool. Fang et al. [53] also studied the tool geometry effects on tool wear. They tested different tool types such as two-flute end mills, triangle-based end mills and semicircle-based (D-type) end mills as shown in Figure 2.4. Among all, D-type end mills are found out to be most rigid one and showed better cutting performances. Bao and Tansel [54] investigated the tool run-out effects on cutting forces. They observed that tool run-out causes force fluctuations which can be avoided either by using collet-type tool holders or aligning tool cutting edges carefully with the setscrew at 90°.

For micro end mills, Aurich et al. [54] proposed a new geometrical with the aim of producing tools which provide good chip formation and removal, cause low cutting forces and friction with newly formed surfaces. Torres et al. [55] analysed the performance of different coatings on micro end mills. They concluded that diamond coatings decrease friction and chemical inertness especially

for Aluminum. Uhlmann and Schauer [56] conducted dynamic load and strain tests on micro end mills and presented a new geometry. Cheng et al. [57] also designed and developed micro straight edge end mills to machine hard and brittle materials.

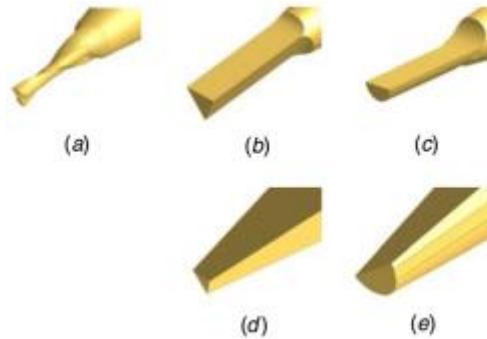


Figure 2.4 - (a) Two-flute end mills, (b) Triangle type end mills with a straight body, (c) D-type end mills with a straight body, (d) triangle type end mills with a tapered body, and (e) D-type end mills with a tapered body

There are also some important studies on tool deflection. The effects of tool deflection in conventional milling can be neglected for some cases. However, for micromilling operations, tool deflection causes noticeable problems such as ruined surface forms. In order to avoid ruining surface quality, there are many studies in literature on the modelling of tool deflection. Depince et al. [55] tried to compensate tool deflection errors by using mirror method. Another model by Zeroudi et al. [56] is a FE Model which also compensates tool deflection by using mirror method. Another FE model by Mamedov [57] has been developed which estimates the instantaneous deflection of the tool by taking cutting forces as distributed loads on flutes. Geometrical models have been developed by Larue [58] and Ryu [59] which estimate form errors in sidewall machining.

One of the most popular models of tool deflection include cantilever beam model. Kim et al. [60] predicted tool deflection and three-dimensional error with cantilever beam representation. Rao and Rao [61] also used cantilever beam model and compensated surface errors. For force estimation, they used a mechanistic approach. Rodriguez and Labarga [62] considered the tool as a cantilever beam, too and they examined tool deflection effects on cutting forces. In their instantaneous chip thickness calculations, they've added the effect of tool deflection.

2.8 Process Parameters

A research on adjusting spindle speed, feed rate and depth of cut to achieve maximum MRR is conducted [18]. They observed that higher MRR can be obtained at medium cutting speed, high feed rate and depth of cuts.

Cutting speed, feed per tooth, axial and radial depth of cut are tested in a research [66] to investigate their effects on tool life while side milling of Ti-6Al-4V with a cemented carbide tool. Among all, cutting speed has the greatest influence on tool life, followed by depth of cuts. At small depth of cuts, friction between the tool and the workpiece increase, leading to heat generation and tool wear. The tools in micromilling generally undergo a sudden breakage due to the increasing cutting forces rather than wearing in time [9]. Additionally, tool wear rate can increase if the cutting temperature increases, for this reason, cutting temperature should be kept under control. Cutting temperature can be controlled by adjusting cutting parameters to reduce the friction and also by lubricants. Effects of cutting conditions such as lubricant types are also experimented and it is resulted that the misting rather than flooding provides a longer tool life and 2210 EP mist shows better results than blasercut mist [14].

It is experimented on a titanium alloy that the most effective cutting parameter on surface roughness, R_a , is the feed per tooth, f_t [67]. When the f_t is increased, surface roughness decreases as half of the case when the spindle speed or the axial depth of cut is increased. Thus, clearly f_t is determined as the dominant effective parameter for the surface roughness. They concluded that the lowest surface roughness is the outcome of the process with the high spindle speeds and feeds, and medium axial depth of cuts. In another research [23], surface roughness is observed to be the lowest at small tool edge radius and high feed rates. For aluminium, it is experimented that when the depth of cut is increased, surface roughness increases [27]. The reason can be shown as the increase in the depth of cut, also increases the cutting forces, which causes tool to be deflected and surface roughness to get worse. On the other hand, it is also observed that the increase in the cutting speed provides better surface quality up to a point, bounded by the vibration formation.

Burr formation is a critical consequence in micromilling which affects the surface quality and geometrical accuracy. Generally, burr sizes are bigger at the entrance and at the exit way of the

tool. Workpiece material and tool geometry can provoke favourable condition for burr formation, however cutting parameters can also lead to important burr development. As mentioned earlier, the large tool edge radius-to-chip load ratio significantly increases burr sizes. In a study [67] examining the effects of spindle speed, axial depth of cut and feed per tooth on burr formation for a titanium alloy, axial depth of cut is found to be the slightly higher effective parameter compared to other parameters. They achieved lowest top burr sizes at high spindle speed and axial depth of cut, and low feeds. For aluminium, it is observed that the spindle speed has a decreasing effect on burr formation [27]. When the same test are applied on a stainless steel workpiece, similar to aluminium, it is observed that the increase in the feed and the cutting speed provide smaller burrs, and the increase in the cutting depth caused high burr formation. However, as a material, stainless steel caused less burr formation than aluminium due to its lower ductility.

It can be concluded that, for burr formation mechanism, ploughing is an important phenomenon. Change in parameters that increase ploughing, such as a decrease in feed rate, also increases surface roughness and burr formation. As the feed rate increases, ploughing is lowered, so as the surface quality gets better and less burrs form. For the ductile materials, minimum chip thickness value is higher. Burr formation and higher surface roughness are observed at lower chip thicknesses. Increase in the axial depth of cut deteriorates the burr formation and the surface roughness.

Cutting force is directly affected by many cutting parameters such as feed per tooth, cutting speed, depth of cut, hone radius and helix angle [68]. As mentioned earlier, due to the trochoidal path of the tool, chip thickness varies during the material removal process. As the chip thickness changes, cutting force also changes accordingly.

Another variable that should be considered for the development of milling performances is the tool geometry. The most effective parameters regarding the tool geometry are the cutting edge radius, helix angle and the number of the flutes. It is found out that the decrease in the flute number of the tool or the decrease in the helix angle increases the cutting forces and the surface roughness, and it also creates a more non-uniform surface topography [69]. As the flute number or helix angle increases, the volume of the tool in the workpiece goes down, which provides a uniform topology. It is also found out that the most dominant parameter effecting the average surface roughness, R_z ,

is the tool run-out. The effect of the rake angle and the relief angle is found to be less effective but in a complex relation [70]. At the low relief and helix angles, process performance is high. When the relief angle is high, better performances are achieved at high helix angles. Tools with variable helix angles are very important to observe better performances. These tools are mostly designed to enhance chatter stability. Also, tool side edges can be tapered to increase side edge angles. When the side edge angles are increased, it is observed that the burr sizes are reduced [71].

2.9 Multiple Objective Optimization Methods

Multi-objective optimization is used in problems when there is more than one objective with contradicting optimal solutions. For an optimization of a micromilling process, minimal cost, maximal quality, in a minimal time requires different optimal solutions, some of which sacrifices one objective over the other. Thus, determining cutting parameters for specified objectives can be treated as a multiple objective problem.

For multiple objective optimization problems, there is no single solution satisfying all the objectives simultaneously. A better solution exists in the solution set, which optimizes a specific objective while degrading another one. Therefore, set of relatively better solutions are tried to be found which is called Pareto optimal solutions or non-dominated solutions [63]. In Pareto optimal solution set, none of the optimal solutions dominate each other, but the optimal solution is chosen by a decision maker (DM), considering the priority of the objectives. Multiple objective problems are found in the general form as [64];

$$\begin{aligned}
 &\text{Minimize/Maximize} && f_m(x), && m = 1, 2, \dots, M; \\
 &\text{subj. to} && g_j(x) \leq 0; && j = 1, 2, \dots, J; \\
 &&& h_k(x) = 0; && k = 1, 2, \dots, K; \\
 &&& x_i^{(L)} \leq x_i \leq x_i^{(U)}; && i = 1, 2, \dots, n.
 \end{aligned} \tag{2.1}$$

where $f_m(x)$ is the objective function which can be aimed to be minimized or maximized, x is the decision variable in the feasible set of $X = (x_1, x_2, \dots, x_n)^T$, $g_j(x)$ and $h_k(x)$ are the constraints to be satisfied by the solutions, and finally $x_i^{(L)}$ and $x_i^{(U)}$ are the lower and upper bounds

consecutively. These bounds represent the lower and upper limits that values should take due to the physical or mechanical limitations.

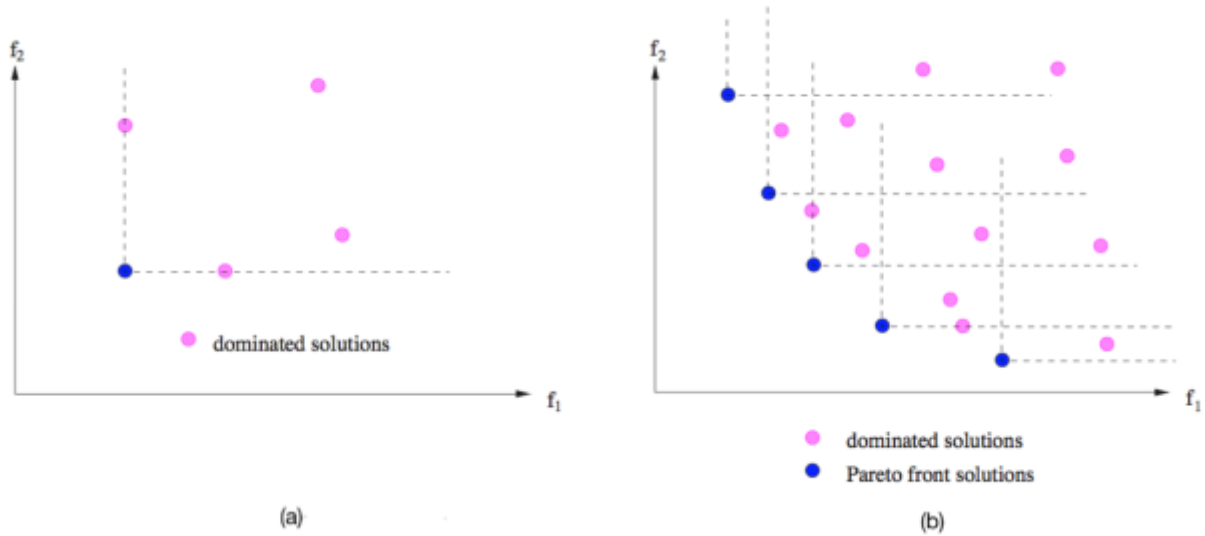


Figure 2.5 - (a) Dominated solution in two objective space; (b) The Pareto front of a solution set in two objective space [65]

If there is no other solution dominating the vector, x , then x is a Pareto optimal solution. MOOPs methods try to achieve Pareto optimal solutions, then decision maker chooses the solution according to preference weights of the objectives.

It is hard to achieve Pareto optimal solutions if the solutions are distributed non-continuously or in non-convex spaces [66]. In many engineering problems, discontinuous solution sets exist. There are many different methods to solve for the solution sets such as weighted methods (weighted sum, weighted min-max, weighted product, exponential weighted), goal programming methods, bounded objective methods, ϵ -constraint methods, meta-heuristic/stochastic methods etc.

Methods to solve MOOP can be classified as no preference methods, a priori methods, a posteriori methods and interactive methods. These classification is done regarding the decision making process. In no preference methods, there is not a decision making step among the solution set. In a priori methods, which are commonly used before 1900s, preference information is defined beforehand and then the better solution is chosen accordingly. Weighted sum methods, ϵ -constraint method, weighted metric method and goal programming are types of a priori methods. In each run,

these methods find one Pareto optimal solution. These methods generally convert the multiple optimization problem into single optimization problem and then use deterministic or stochastic methods to give solutions. In posteriori methods, which are commonly proposed after 1900s, DM chooses the preferred solution from the set of Pareto optimal solutions. These methods find many Pareto optimal solutions in one run. A posteriori methods consist of mathematical programming based methods and evolutionary algorithms. Mathematical methods can be subdivided into normal boundary intersection (NBI), modified normal boundary intersection (mNBI), normal constant (NC) etc. and evolutionary algorithms can be subdivided into multi objective generic algorithms (MOGA), non-dominated sorting generic algorithm-II (NSGA-II), strength Pareto evolutionary algorithm 2 (SPEA-2), particle swarm optimization (PSO) etc. In recent years, these methods are very popular due to their ability to achieve many Pareto optimal solutions in one run, and having no need to make assumptions on the objective functions [67]. In interactive methods, DM guides the Pareto optimal solutions by making preferences at each iteration. Additionally, hybrid models are generated by merging different algorithms.

In literature, multiple objective optimization methods are used in many different areas including micromilling process optimization. Jithin et al. [68] used generic algorithm on MATLAB to maximize MRR and minimize tool wear rate in micro ED milling. Studies in micromilling includes Yang et al. [69], who used generic algorithm (GA) for simultaneously decreasing the production cost and the production time. They determined the machine power, cutting force, machining speed, feed rate and the surface roughness as their constraints. Li et al. [70], optimized two objectives in micro end milling; the first one is to minimize production time and consumed tools, second one is to minimize production time, surface roughness and the residual stress. They used NSGA-II and minimized the values by 5%. Natarajan et al. [2] worked on achieving the maximum MRR and minimum surface roughness in micromilling using response surface methodology. Deb et al. [71] compared the methods and stated that NSGA-II performs better results than strength pareto evolutionary algorithm (SPEA) and pareto archived evolution strategy (PAES).

Jha [72] used geometric programming (GP) and resulted that the GP is time-consuming. Wang et al. [73] developed a hybrid algorithm, combining GA and simulated annealing (SA) and optimize

machining parameters. By the help of local selection strategy of SA, they were able to eliminate premature convergence of GA.

As stated earlier, MOOP methods generally converts the problem into single objective optimization problems. The conversion creates problems when the solutions are distributed discontinuously or in a non-convex area [74]. In recent years, particle swarm optimization (PSO), developed by Kennedy and Eberhart [75], is widely used in engineering problems due to its simplicity and efficient computing. It has a unique searching mechanism which gives feasible solutions for engineering optimization problems.

PSO became popular in recent years, especially it is a very successful algorithm for the solutions of the problems with the real decision variable values [65]. The reasons why PSO became so popular can be summarized as: first, it has a simple logic and easy implementation to different problems; second, it has ability to give very good results in a short time [65]. It can be implemented to many different areas. There are many implementations of PSO to milling optimization problems in recent years. Natarajan et al. [2] used PSO to optimize cutting parameters and predict tool life. Thepsonthi and Ozel [76] also used PSO to find optimum parameters for minimum surface roughness and burr formation. In his dissertation, Thepsonthi [77] chose PSO to optimize micromilling process due to its efficiency and easy implementation, as he stated. Yang et al. [69] used PSO on a fuzzy global and personal best mechanism, which is called F-MOPSO. This algorithm avoids data clustering and therefore provides more effective results. In the study, researchers considered the statement by Deb et al. [71], which indicates the superior performance of NSGA-II, and compared PSO with the solutions they achieved by using NSGA-II. In the case studies they have made, they concluded that the NSGA-II failed to cover all Pareto optimal solutions and also gave solutions which are not true. For the all case studies, F-MOPSO performed better than NSGA-II.

2.10 Objective and Motivation

The objective of this study is to optimize micro end milling process parameters with the purpose of production time and cost minimization considering surface roughness, burr formation and cutting forces. By using MOPSO algorithm, multiple objectives are minimized for better production performance and part quality. Tool geometry and some parameters for the part to be machined are entered as an input to the algorithm. The algorithm calculates surface roughness, burr size and cutting forces for each combination of random cutting parameters and keeps them in acceptable limits while minimizing production cost and time. The output of the algorithm is a Pareto curve of minimized objective function values and solution set of decision variables, which are determined as the cutting speed, feed rate and depth of cut, which are the most effective parameters on constraints. These decision variables are selected depending on the previous studies presented in the previous section.

Many studies have been conducted on micromilling process optimization. These studies generally aim to minimize or maximize a certain criterion such as surface roughness or burr height. There are also multiple objective optimizations using some other techniques. This study is the first implementation of MOPSO algorithm on micromilling. It is also the first time of multiple objective optimization considering many constraints, offering a full solution for better production performance and part quality.

3. UNIQUE MECHANISMS OF MICROMILLING

3.1 Fundamentals

In today's industry, micromilling is a rapidly emerging manufacturing process on account of its high precision capability and wide applicability in various industries. Micromilling can be used to manufacture high strength workpiece materials with complex geometries in tight dimensional tolerances where other micro machining techniques (additive manufacturing, lithography etc.) cannot be used. Furthermore, micromilling has much higher material removal rate and it is a flexible manufacturing method for customized products compared to other micro machining processes.

Conventional milling is a familiar production process which is the shaping of the workpiece with a rotating cutting tool by removing chips. In micromilling process, tools, workpiece and the target product details are scaled down by ~1%. As the process precision is increased compared to conventional milling, researchers try to highlight kinematics, dynamics and thermal effects of chip formation in micromilling and how they are affected by the size reduction. Since tool failure is a common problem in micromilling, modelling of the process, selection of the tools and the parameter carry a crucial role. Proper selection of tool geometry, cutting speed, depth of cut and feed rate will provide improved tool life, surface roughness, cutting forces, burr formation, process time and cost.

Micro end milling is generally used in the machining of metals and polymers. Hard to machine metals and their alloys are widely used in miniaturized geometries. Materials with biocompatibility such as titanium alloys and steel have a popular usage in medical industry. Titanium alloy is also widely used in aeronautical materials due to their high stiffness, oxidation and corrosion resistance. However, titanium alloys have low thermal conductivity; when heat is generated during the cutting process, it is hardly dissipated from the workpiece. Rapid tool wear and geometrical accuracy become a significant problem. Aluminium is also a common workpiece material for micromilling applications. Even though aluminium is a soft metal, because of its high ductility, burr formation is very high. Thus, it is hard to obtain good surface finish when machining aluminium.

There are various types of micromilling tool geometries including end mills, ball-nose mills. Tool cutting edge has a significant effect in micromilling since the cutting edge radius has a notable value (normally 1-5 μm) due to miniature geometries. Tool materials are commonly tungsten carbide or diamond and different types of coatings exist such as TiAlN, AlCrN, TiCN, ZrN etc.



Figure 3.1 - Nanofocus image from a flute of a 2mm micro end mill

3.2 Minimum Chip Thickness and Ploughing Effect

The major difference between conventional milling and micromilling arises from the size reduction, as noted before. The relation of process geometry and tool geometry changes considerably. With the micro tools having diameters less than 1mm, tool breakage under high chip loads are frequently encountered. To avoid tool breakage, chip thickness in micromilling are generally few hundreds of microns. Since the uncut chip thickness, t_0 is very small; tool edge radii, r_c , cannot be ignored. So the tool is not considered ‘sharp’ as in conventional milling, as shown in Figure 3.2 and the contact is analysed between the tool and the clearance face of the workpiece.

Under a critical uncut chip thickness value, the material is compressed under the tool and no chip forms. After tool passes, it recovers back, so only elastic deformations exist [78]. In this case, the shear energy and the cutting force are very high. Right at the critical value, which is denoted as minimum chip thickness, t_c , tool starts to remove chips from the workpiece by mechanical shear force [79]. Still, there is elastic recovery in some portion. When the uncut chip thickness is higher than the minimum chip thickness, the material is removed as a chip.

When the uncut chip thickness value is below minimum chip thickness, only ploughing force exists. To investigate chip formation and ploughing effect, the ratio of minimum chip thickness to the cutting edge radius (hone radius) is taken as a basis. As the tool gets sharper, chip formation starts at lower minimum chip thickness values. Thus, if the aim is to remove a very thin layer from the workpiece, the tool needs to be as sharpest as possible, which is limited due to the tool production limitations and to the grain sizes. When the tool edge radius is higher, ploughing occurs at smaller chip thickness values. A study shows that the minimum chip thickness values ranges approximately between 20-40% of hone radius [25]. Ploughing force increases together with the cutting forces and surface roughness. Large burrs and tool wear are observed due to ploughing force, which is unwanted [20] [21].

Due to very low uncut chip thickness, another phenomenon emerged is the negative rake angle. When the ratio of minimum chip thickness-to-hone radius is equal or less than 1, the rake angle becomes negative. Negative rake angle leads to multiple material phases during the cutting process [80]. Existence of negative rake angle has significantly affects the cutting process which brings necessity to consider springback. Liu et al [81] stated that the size reduction in micromilling affects the cutting force, chip thickness, chip formation and surface quality.

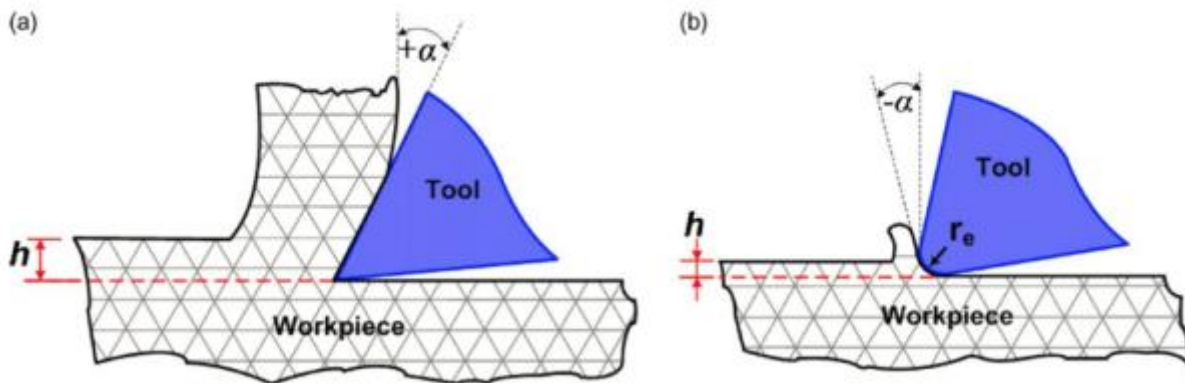


Figure 3.2 – (a) Macro-milling; (b) Micromilling [1]

On the other hand, size effect also changes the relation between the process geometry and grain. Due to the size reduction and sensitivity of the process and the tool, grain structures cannot be

neglected too. An average uncut chip thickness can have the same size with a grain as demonstrated in Figure 3.2. In this case, as it is much convenient to consider the process homogeneous in conventional milling, heterogeneity of the process comes forward in micromilling. When the tool is removing grains as it moves, due to the heterogeneity of the grain structure, cutting force fluctuates in time.

The uncut chip thickness to the tool cutting edge radius is essential in micromilling for the chip formation processes. For a chip formation without ploughing effect, the ratio of minimum chip thickness-to-hone radius needs to be above 1, in order to have a positive rake angle. When the rake angle is negative, ploughing force exists, which causes higher cutting forces and surface roughness.

The value of the ratio is examined in many researches for micromilling. Basuray et al. claimed that the ratio needs to be between 0.11-0.16 when the workpiece material is soft aluminium or mild steel. In another research, the ratio of the minimum chip thickness to the hone radius is said to be 1/20 [82]. In other researches, this ratio is agreed to be between %20-%40 [25].

3.3 Chip Removal Process and Consequences

In milling process, during chip removal, chip thickness is variable. As the tool enters the workpiece, the chip thickness increases from 0 to f_t due to the trochoidal path of the tool. Because of the minimum chip thickness phenomenon in micromilling, ploughing takes place at each time a tooth enters the workpiece. Until the tooth reaches the minimum chip thickness value, no chip forms. Consequently, as tool moves, it leaves uncut portions at lateral surface which causes burrs to form.

Ploughing due to minimum chip thickness limitation also has an effect on the basal surface. In consequence of manufacturing capabilities, tools edges cannot be produced as sharp as to neglect hone radius in micromilling. In fact, micro tools have considerable hone radius to chip thickness ratio, as mentioned earlier. Because of the hone radius, tools remove the workpiece at the base in an arc-like profile. Thus, ploughing also takes place at basal surface of the workpiece and chip formation will not occur properly. It is investigated that the newly formed workpiece surface will be affected and formed with elastically deformed uncut material [23]. As the tool moves in a trochoidal path, the following teeth will pass from the newly formed surface by the first cutting

tooth. When the fact that the residual materials will probably be smaller than minimum chip thickness value, following teeth will be lapping the surface material and the surface quality will be affected by the geometry of the cutting process. Plus, tool will be deflected by the excessive force evolving in the cutting direction and the contact geometry of tool entering the workpiece will be changed. As a result, chip profile will change and the friction between the rear tooth and the newly formed surface will diminish.

4. OPTIMIZATION OF MICROMILLING

4.1 Multiple Objective Particle Swarm Optimization (MOPSO)

Particle Swarm Optimization (PSO) is initially proposed by Kennedy and Eberhart in 1995 [85]. It is a population based heuristic global optimization method. Originally, it is modelled on the social behaviours of animals and insects, including bird flocking, fish schooling etc. Later on, the model attracted many attentions from various fields due to its simplicity and efficiency in computing and it is adapted to solving optimization problems.

PSO is one of the evolutionary algorithms. Evolutionary algorithms have three main processes in common [86]. In the first step, they all begin with random initialization of the individuals. In the second step, fitness values for each individual is evaluated. Their next common step is to update individuals and fitness values iteratively. Generic algorithm (GA), particle swarm optimization (PSO) and differential evolution (DE) share these common steps. PSO has computationally advantage over many algorithms. Since the sorting of the fitness values is not required in PSO, it quickly creates the solution. In recent years, PSO is implemented in many difficult optimization problems due to its easy computation and rapid convergence to the optimum [86].

In PSO, each particle is a potential Pareto optimal solution. Iteratively, particles fly towards better fitness values by comparing information from its previous locations and calculating its velocity vector. As the position of particles are updated, the swarm converges around the optimal solutions.

For each particle, the best position it achieved so far is called ‘personal best (*pbest*)’. The best position in the whole swarm is called ‘global best (*gbest*)’. The movement of a particle to its next position is determined by the personal and global best locations. The velocity and the next position of a particle is calculated as follows;

$$x_i(t + 1) = x_i(t) + v_i(t + 1) \tag{4.1}$$

$$v_i(t + 1) = \omega[v_i(t)] + [c_1 r_{i,1}(t) \times (pbest_i(t) - x_i(t))] + [c_2 r_{i,2}(t) \times (gbest(t) - x_i(t))] \quad (4.2)$$

where $i = 1, 2, 3 \dots, n$ represents the particles and t is the iteration number. x_i and v_i give the position and the velocity of the specified particle. Eq. 4.2 is composed of three parts. The first term, which is related to the previous velocity is called ‘momentum’ term. In ‘momentum’ term, ω is the inertia weight; the weightage given to the previous velocity, so this term provides particle movement to be in the direction of the previous velocity. The value of ω can be set to large numbers for the first iteration and decreased in later iterations in order to converge in a small region or it can be given randomly. Generally, if distance between $pbest$ and $gbest$ positions is large, the value of the ‘momentum’ term can be a large value which leads particles to jump over huge distances rather than to converge, even to go beyond the search space. To avoid those cases, velocity clamping method is applied; V_{max} value, which is the maximum velocity that the particle can achieve, is defined [76].

Remaining terms in Eq. 4.2 direct the particle towards $pbest$ and $gbest$ positions. The second term is called ‘cognitive’ term which symbolizes the possibility of a particle to turn back to its previous best positions and the third term is called ‘social’ term which represents the possible movement of a particle towards the other best positions obtained by other particles of the swarm. c_1 and c_2 are the learning factors, and r_1 and r_2 are the random numbers between 0 and 1, which give a stochastic approach to the algorithm [87].

The PSO algorithm starts with defining the population size. Initial positions and velocities are determined randomly. For each particle, fitness values, in other words the objective function values are calculated. In the first step, $pbest$ of each particle is their current position and the $gbest$ is the position of the particle giving the best objective function value. In the next iteration, new position is calculated according to the Eq. 4.1 and Eq. 4.2, the value of the objective function is calculated for the new position of each particle. $pbest$ and $gbest$ are updated with the better positions, if the new positions give better objective function values. The iterations continue repeatedly until the maximum iteration number is reached. In this way, particles converge to optimum values. The iterations in a PSO algorithm can be summarized as follows [87];

Step 1. There are some PSO parameters which need to be defined in the first step. These parameters are the number of particles, dimension of the particles, the maximum velocity that the particles can move, learning factors, inertia weight and maximum iteration value. As the first step, the positions and velocities of the particles are determined randomly. Since they do not have a previous position, *pbest* is set as their current positions. According to their objective function values, *gbest* is chosen and stored.

Step 2. By using Eq. 4.1 and Eq. 4.2 the new positions of the particles are determined and the objective function values are calculated. Accordingly, *pbest* value for each particle is updated with the position with the best fitness value and *gbest* is updated again with the best *pbest* value.

Step 3. All steps are repeated until the maximum iteration is reached.

In PSO, ‘*neighbourhood topology*’ is commonly used. According to the neighbourhood topology, particles are grouped in a local region, from where the particle with the best objective function value is stored as the local best (*lbest*) value. Neighbourhood topology provides better chance to locate global optima of the swarm. Defining the ‘neighbourhood’ varies from algorithm to algorithm but some typical neighbourhood described are; empty graph, fully connected graph, star network, tree network etc. [65]. In their work, Coello Coello et al. [88] used gridification of the workspace to select leaders and stored them in repository.

During the application of PSO to multi-objective optimization problems (MOPSO), there are some issues that need to be considered. One of them is the evaluation of the objective functions. There are two options; objective functions could be combined into one single function or each of them could be evaluated separately for each particle. Secondly, there are particles called ‘*leader*’ which are the guiding particles towards the best positions in the swarm and there are different methods regarding the selection of these particles. Thirdly, those leaders are stored in an external archive and maintaining the archive varies from algorithm to algorithm. Lastly, there is a potential problem for PSO which is the premature convergence into local optimums and maintaining diversity is another key issue [89].

As mentioned previously, particles have leading position (a leader) in their specified neighbourhood topology. In MOPSO, particles may have different leaders and among them, one leader is selected. In order to store the position of the leaders, ‘*external archive*’ is used in MOPSO. In the external archive, all the non-dominated solutions found so far are stored. In order to select a leader from the set of the leaders, ‘*quality measure*’ is defined [65].

As the solution space is getting smaller, the velocities of the particles converge to 0. As a consequence, new solutions cannot be generated and the problem may be trapped in a local optimum. Usually in MOPSOs, cross over and mutation operator is used to overcome premature convergence. By mutating a single particle, the algorithm escapes from the local optima. Either the velocity or the position of a particle can be mutated. Mutation operator is applied after updating the positions of the particles.

The steps used in MOPSO are as follows;

Step 1. All PSO parameters and the initial position of the particles are initialized. A set of leaders is also initialized among the initial particles in an external archive.

Step 2. According to the quality measure, a leader is selected from the external archive and the positions of the particles are updated. Mutation operator is applied and *pbest* values are updated if needed.

Step 3. Leaders are updated and the quality measure is recalculated.

Step 4. All steps are repeated until the maximum iteration is reached.

4.2 Objective Functions

In multi objective optimization problem of micromilling process, as in most of the studies, the objective functions are determined as the production time and production cost which are going to be minimized.

4.2.1 Production Time

Production time is the time spent to produce one single product. It considers the actual machining time (T_m), time wasted without cutting (T_i) and time spent during tool change (T_c) [69].

$$T_{total} = T_m + T_i + T_c \quad (4.3)$$

Actual machining time, T_m depends on material removal rate (MRR). In micromilling, MRR is an important process performance criterion from both researchers' perspective, in order to increase depth of cut limitations for micro tools, and from the manufacturer's perspective, in order to increase production efficiency. For the manufacturer, it is important to achieve low cost production in a short time. MRR is the key performance criteria to achieve this purpose. However, increasing MRR yields more load on the tool, which shortens the tool life. Therefore, there should be an optimum boundary line, to minimize the production cost. MRR is calculated as follows;

$$MRR = \frac{fnad}{1000} \quad (4.4)$$

where d is the tool diameter, a is the depth of cut, f is the feed rate and n is the spindle speed. Production time involves both the roughing time and the finishing time. T_m , T_i and T_c are calculated as the sum of the roughing and finishing operation times as follows;

$$T_m = \sum_{i=1}^n \frac{L_r}{f_r} + \frac{L_f}{f_f} \quad (4.5)$$

where n is the number of the roughing cycles, L_r and L_f are the travel lengths for roughing and finishing operations, and f_r and f_f are feeds for roughing and finishing operations.

$$T_i = T_p + n(h_1 L_r + h_2) + (h_1 L_f + h_2) \quad (4.6)$$

where T_p is the setup time, h_1 (minutes per millimeter) and h_2 (minutes) are the constants related to tool movement before and after cutting.

$$T_c = T_{tc} \sum_{i=1}^n \frac{L_r/f_r}{T_{life}} + \frac{L_f/f_f}{T_{life}} \quad (4.7)$$

where T_{tc} is the tool change time and T_{life} is the tool life.

4.2.2 Production Cost

Similar to the production time, unit production cost is calculated combining the actual machining cost (C_m), machining idle cost (C_i), cost during tool change (C_c) and the tool cost (C_t) [69]. Labour and overhead costs are included in the constant, k_0 (dollars per minute) and k_t (dollars per tool) is the unit tool cost.

$$C_{total} = C_m + C_i + C_c + C_t \quad (4.8)$$

$$C_m = k_0 T_m \quad (4.9)$$

$$C_i = k_0 T_i \quad (4.10)$$

$$C_c = k_0 T_c \quad (4.11)$$

$$C_t = k_t \sum_{i=1}^n \frac{L_r / f_r}{T_{life}} + k_t \frac{L_f / f_f}{T_{life}} \quad (4.12)$$

Tool cost, C_t depends on tool life. For the process optimization, tool life maximization is one of the main purposes. Especially for micromilling, micro tool production is much costlier and tools are much more fragile compared to conventional milling, thus tool life maximization is even more essential.

As ploughing mechanism is a common phenomenon in micromilling, tools often fail due to progressive wear or over chipping. When tool material goes through plastic deformation, tool is sorted as 'worn' [90]. As the tool wears, heat is generated and the surface roughness increases which is very undesirable if high precision production is intended. So, the tool life ends when tool wear is above a threshold value.

Recent studies mostly depend on experimental curve fitting implications to a very earlier and well-known modelling of Taylor [11]. Taylor defines tool life as follows;

$$VT_{life}^n = C \quad (4.13)$$

where T_{life} is the tool life (min), V is the cutting speed (m/min), n and C are the constants. According to the process conditions, such as dry/lubricated cutting, cutting parameters, workpiece and tool materials, geometries, the constants vary.

4.3 Constraints

As mentioned previously, high accuracy and part quality is demanded from micromilling operations. Because of this, for the multiple objective optimization problem of micromilling, the constraints are selected as the surface roughness, burr height and cutting forces. Solution set is determined under acceptable values for these constraints.

4.3.1 Surface Roughness

In micromilling, surface quality is the one of the main objectives. Since the purpose in micromilling materials is to produce miniature parts with complex geometries and high geometrical accuracy, minimization of surface roughness is one of the focal topics. There are many factors effecting surface roughness; from process strategies to cutting tool geometry, from CNC machine precision to process parameters.

Surface roughness models carry an important role in order to predict process parameters and outcomes in advance. There are many studies on surface roughness in macro-milling. As mentioned earlier, micromilling process have different process dynamics than conventional milling, like ploughing effect or the hone radius-to-minimum chip thickness ratio. Thus, these models are inapplicable.

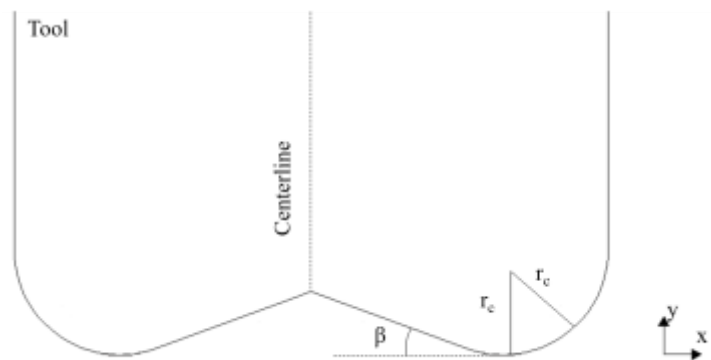


Figure 4.1 - Cutting tool profile in micromilling [23]

In literature, there are some studies regarding to the surface formation in micromilling. It is proven that the dominant parameter effecting the surface roughness is the minimum chip thickness [23]. It is found out that the better surface quality is achieved in the single phase materials, ferrite and pearlite than the multiphase materials. In the study, the surface formation is modelled considering the geometry of the micro tool, as in Figure 4.1, and the effect of minimum chip thickness on the surface formation. As mentioned earlier, in micromilling, chip thickness should be above a certain value, which is stated as ‘minimum chip thickness’, in order for tool to remove chips from the workpiece. If not, tool will cause elastic and plastic deformations on workpiece. As the tool passes, elastic and plastic deformations may occur at previously formed surfaces since the chip thickness will be lower than the uncut chip thickness, and the chip will form from the parts that the chip thickness is above the minimum chip thickness value. Thus, final surface profile will be a combination of the previously formed surface and the newly cut surface. The tool profile is described as follows [27];

$$y(x) = \begin{cases} -\sqrt{r_c^2 - x^2}; & x > -r_c \sin \beta \\ -r_c \cos \beta - [x + r_c \sin \beta] \tan \beta; & x \leq -r_c \sin \beta \end{cases} \quad (4.14)$$

In a recent study [27], surface roughness is modelled considering the bottom surface formation. The parameters considered during modelling are the tool geometry, feed rate and the minimum chip thickness. Other parameters, like cutting speed and depth of cut, are accepted as they are dominantly effecting the material behaviour in terms of heat generation and material deformation. Thus, these parameters will be determining the minimum chip thickness value.

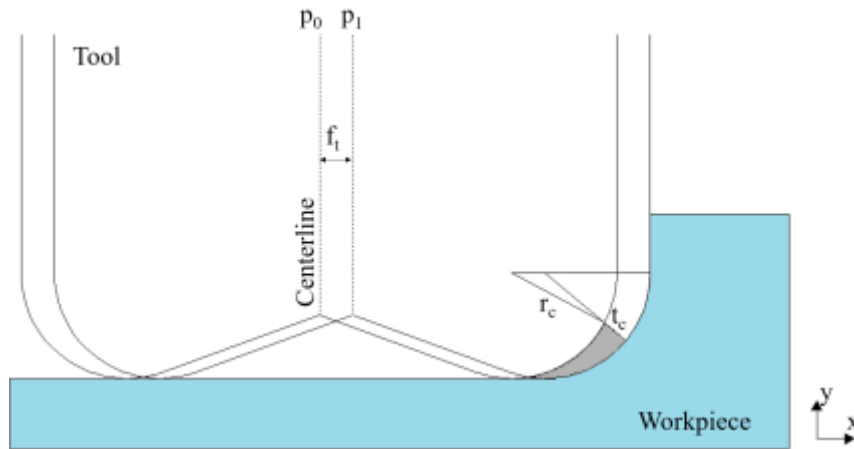


Figure 4.2 - Material removal process in trochoidal tool path

Considering the tool geometry in Figure 4.1, chip thickness will vary due to the hone radius. Volume of the material removed will be as in as the tool moves in a trochoidal path. As a result of the minimum chip thickness concept and the hone radius, during chip removal, some of the material will be removed, but some of them will undergo plastic deformation where chip thickness is below the minimum chip thickness, t_c , as shown in Figure 4.2.

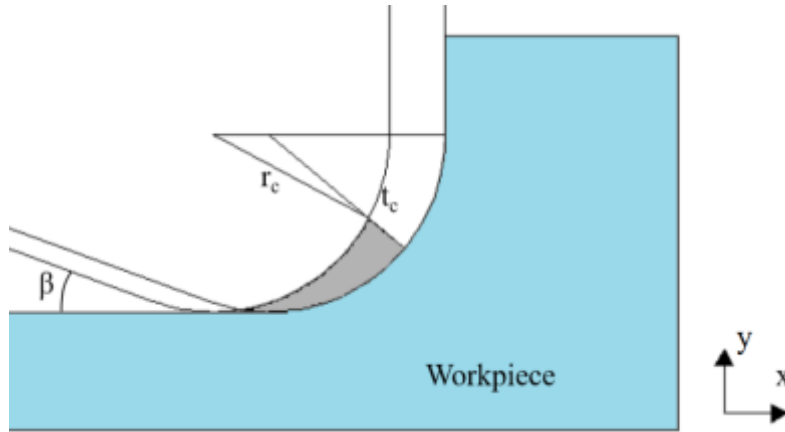


Figure 4.3 – Minimum chip thickness and plastically deformed area

The angle between the x-axis of the tool hone center and the borderline separating the two regions (where the chip could be removed and where the chip could not be removed) is called rake angle (see Figure 4.3) and calculated as follows [27];

$$\alpha = \cos^{-1} \left(-\frac{(r_c - t_c)^2 - f_t^2 - r_c^2}{2f_t r_c} \right) \quad (4.15)$$

As the tool moves in $x+$ direction at f_t , the area under the minimum chip thickness border which is going to be plastically deformed is built up as shown in Figure 4.4. Since the location of t_c borderline depends on f_t value, for the cases $f_t < t_c$, no chip will form. As the tool moves, chip thickness value is reached, and the chip begins to form, as shown in Figure 4.4.

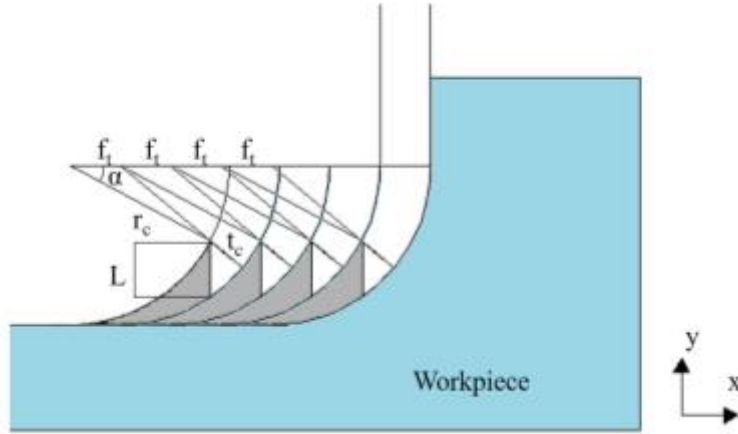


Figure 4.4 - Case 1: $f_t < t_c$

By periodically calculating the area under the tool, surface profile can be described as follows [27];

$$y_{profil} = \begin{cases} y = r_c - \sqrt{r_c^2 - x^2} & 0 < x \leq r_c \cos \alpha \\ y = r_c - \sqrt{r_c^2 - x^2} & r_c \cos \alpha < x \leq f_t n_{ft} + r_c \cos \alpha \end{cases} \quad (4.16)$$

where n_{ft} defines the number of the tool step at feed rate when the chip formation begins.

As mentioned earlier, there are different measurements used to identify surface roughness degree. One of the methods is the distance between the minimum and the maximum surface levels, R_t , which is shown in Figure 4.4. R_t can be calculated by the geometrical relation as follows [27];

$$R_t = r_c - \sqrt{r_c^2 - (r_c \cos \alpha)^2} \quad (4.17)$$

For the cases $f_t > t_c$, the bottom edge of the tool also contacts to the workpiece. As it can be seen in Figure 4.5, the tool has hone radius continuously in an arc profile. The arc profile corresponds to an angle of $90^\circ + \beta$. Because of the tool geometry, bottom edge of the tool also has a contact with the workpiece. Thus, minimum chip thickness phenomenon will also be valid for the area at the bottom.

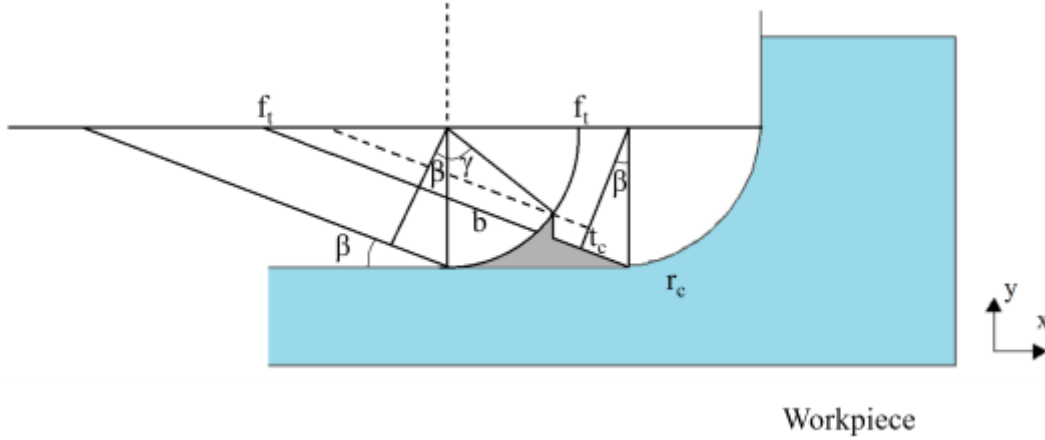


Figure 4.5 – Case 2: $f_t > t_c$

The angle, γ gives the boundary of the residual material at the bottom. The angle and the surface profile can be calculated as follows [27];

$$\gamma = \cos^{-1} \left(-\frac{(r_c - \sin \beta f_t - t_c)^2 - b \cos(90 + \beta)}{r_c} \right) \quad (4.18)$$

$$y_{profil} = \begin{cases} y = r_c - \sqrt{r_c^2 - x^2} & 0 < x \leq r_c \sin \gamma \\ y = r_c - \sqrt{r_c^2 - x^2} & r_c \sin \gamma < x \leq f_t \end{cases} \quad (4.19)$$

The distance between the maximum and minimum surface levels (R_t) can be calculated as follows [27];

$$R_t = r_c - \sqrt{r_c^2 - (r_c \sin \gamma)^2} \quad (4.20)$$

4.3.2 Burr Height

During milling process, there may be some cases that workpiece material could not be removed as chips, but it sticks to the edges or to the surface, outside the target geometry. In micromilling, burr formation is unacceptable for high precision products. Unfortunately, burr formation is unavoidable and manufacturers are contented to reduce burr sizes to an acceptable value. To reduce burr size, researchers try to optimize influent conditions such as material properties, tool geometry

and the cutting parameters. There are different burr size evaluation criteria; burr size can be defined by measuring burr height, burr width, burr thickness, burr volume or burr hardness, in some cases.

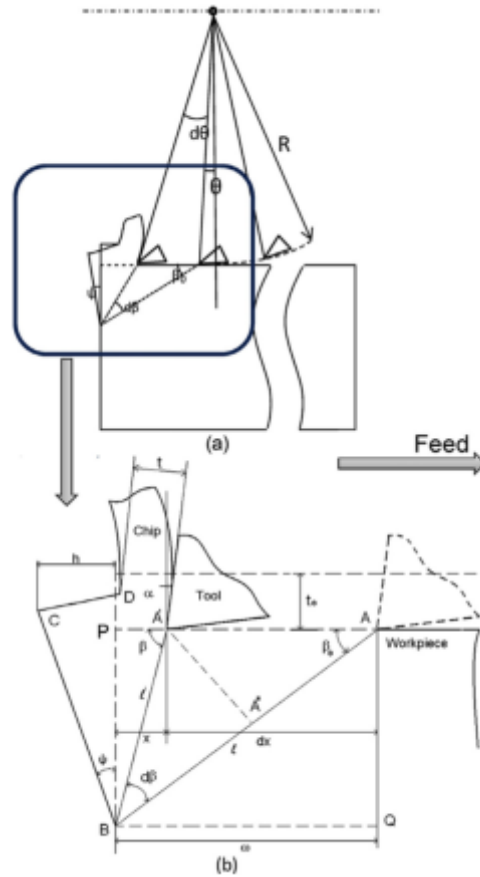


Figure 4.6 – (a) Exit geometry in micromilling; (b) Geometry of burr formation [28]

In literature, modelling of burr height is done through empirical formulations and curve fitting. A recent study by Kumar et al. [91] developed a mathematical model for predicting exit burr size in the micromilling of Ti6Al4V. They achieved a very small prediction error, 3%. They were able to reduce burr size by 90% by adjusting the cutting speed. Their model is based on the geometrical calculations made by Ko and Dornfeld [28], who defined the burr height in micromilling as follows;

$$h_f = (t_0 + \omega \tan \beta_0) \cos \beta_0 \quad (4.21)$$

From Figure 4.6, the triangles $AA'B$, APB and $A'PB$ give the following relations;

$$AA' = R d\theta = l' d\beta \quad (4.22)$$

$$PB = l' \sin \beta = \omega \tan \beta_0 \theta \quad (4.23)$$

which can be written as;

$$l' = \frac{\omega \tan \beta_0}{\sin \beta} \quad (4.24)$$

where θ is the tool rotation angle, β is the negative shear angle, β_0 is the initial negative shear angle and $d\theta$ and $d\beta$ are very small angles. If Eq. 4.24 is substituted into Eq. 4.22, ω , which is the initial tool distance from the workpiece, can be solved as;

$$\omega = - \frac{R\theta}{\log\left(\frac{\tan \beta_0}{2}\right) \tan \beta_0} \quad (4.25)$$

where R is the tool radius. Kumar et al. [91] used the mathematical chip thickness modelling of Y. H. Kang [92];

$$t_c = t_x \sin \theta - \frac{N t_x^2 \cos \theta \sin \theta}{2\pi R + N t_x \cos \theta} + R - \sqrt{R^2 - \left(\frac{2\pi R t_x \cos \theta}{2\pi R + N t_x \cos \theta}\right)^2} \quad (4.26)$$

where t_c is the chip thickness and t_x is the feed per tooth. Since Kumar et al. [91] investigated burr formation at the exit, they took the tool rotation angle, θ as 0 and simplified the formulation and rewrite the model of Ko and Dornfeld [28] as;

$$t_0 = t_x \theta - \frac{N t_x^2 \theta}{2\pi R + N t_x} + R - \sqrt{R^2 - \left(\frac{2\pi R t_x}{2\pi R + N t_x}\right)^2} \quad (4.27)$$

$$h_f = \left[t_x \theta - \frac{N t_x^2 \theta}{2\pi R + N t_x} + R - \sqrt{R^2 - \left(\frac{2\pi R t_x}{2\pi R + N t_x}\right)^2} - \frac{R\theta}{\log\left(\tan \frac{\beta_0}{2}\right)} \right] \cos \beta_0 \quad (4.28)$$

In their work, Ko and Dornfeld [28] stated that the work done for burr formation is equal to work done to remove chips. Principle of continuity of work is given below;

$$\Delta W_c = \Delta W_b \quad (4.29)$$

$$\Delta W_c = \frac{bt_x K_t}{4\pi} [4\pi R + \pi t_x \theta - N t_x \sin \theta \sin \theta + \pi \cos \theta (t_x \sin \theta - 4R)] \quad (4.30)$$

$$\Delta W_b = \int_0^\theta \left(\frac{k_0}{2} \cos \beta_0 \cos \beta_0 + \frac{\sigma_e}{4} \tan \beta_0 \right) \omega R d\theta = \left(\frac{k_0}{2} \cos \beta_0 \cos \beta_0 + \frac{\sigma_e}{4} \tan \beta_0 \right) \omega R \theta \quad (4.31)$$

where K_t is the specific tangential cutting pressure, b is the plunge depth, k_0 is the yield shear strength and σ_e is the normal yield strength. From Von-Mises criterion, $k_0 = \frac{\sigma_e}{\sqrt{3}}$. By substituting the value of k_0 from Von Mises criterion and the value of ω from Eq. 4.26, and the formulations for ΔW_c and ΔW_b from Eq. 4.31 and Eq. 4.32 into Eq. 4.30, the following equation is obtained whose roots give the solution for the tool rotation angle, θ ;

$$\frac{bt_x K_t}{4\pi} [4\pi R + \pi t_x \theta - N t_x \sin \theta \sin \theta + \pi \cos \theta (t_x \sin \theta - 4R)] + \frac{0.0126R^2 \theta^2}{\log(\tan \beta_0 / 2) \tan \beta_0} \left(\frac{\sigma_e}{2\sqrt{3}} \cos \beta_0 \cos \beta_0 + \frac{\sigma_e}{4} \tan \beta_0 \right) = 0 \quad (4.32)$$

The burr height can be calculated from Eq. 4.28 and Eq. 4.32 [91].

4.3.3 Cutting Forces

In micromilling, cutting force is significant in terms of the tool life and surface quality due to the excessive heat generation. Modelling of cutting forces enable to achieve better surface performances regarding longer tool life and smoother surface. There are many different aspects to force modelling. Later studies adapt the slip-line theory, which is basically dividing the workpiece into sub-regions where different deformation mechanisms take place. As mentioned previously, chip thickness varies as the tool enters the workpiece. This variation depends on the immersion angle value. The variation of the chip removal has a periodic repetition which is described as [93];

$$h(\phi) = f_t \cdot \sin \phi \quad (4.33)$$

where f_t is the feed per tooth (mm/rev.tooth) and ϕ is the instantaneous immersion angle. As the immersion angle changes, different combinations of ploughing and chip removal mechanisms take place. According to the slip-line theory, the workpiece is divided to three regions; primary, secondary and third deformation zones.

A recent study uses thermo-mechanical approach to model cutting forces in micromilling which is going to be presented in this section. The study also includes bottom forces involving in the cutting process [3].

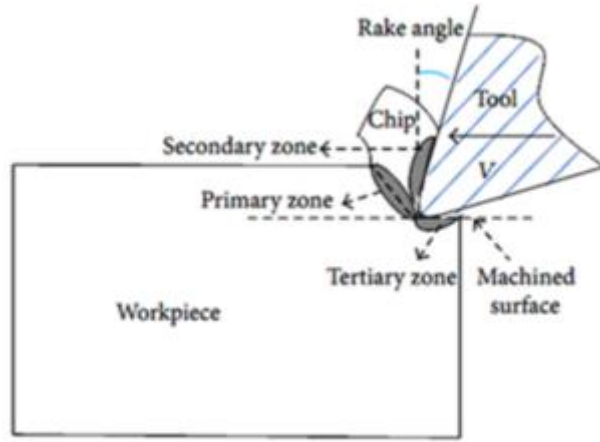


Figure 4.7 - Primary, secondary and tertiary deformation zones

4.3.3.1. Primary Deformation Zone

The primary deformation zone is modelled according to the Johnson-Cook model as follows [94];

$$\tau = \frac{1}{\sqrt{3}} \left[A + B \left(\frac{\gamma}{\sqrt{3}} \right)^n \right] \left[1 + \ln \left(\frac{\dot{\gamma}}{\dot{\gamma}_0} \right)^m \right] \left[1 - (\bar{T})^v \right] \quad (4.34)$$

where γ is the shear strain, $\dot{\gamma}$ is the shear strain rate, $\dot{\gamma}_0$ is the reference shear strain rate. A, B, n, m and v are the material constants. The reduced temperature, \bar{T} can be calculates as follows;

$$\bar{T} = \frac{(T - T_R)}{(T_M - T_R)} \quad (4.35)$$

where T, T_R, T_M represent the absolute temperature, reference temperature and the melting temperature consecutively. Shear stress at the entrance and at the exit of the primary deformation plane is represented by τ_0 and τ_1 consecutively, and their relation can be calculated iteratively by [94];

$$\tau_1 = \rho(V \sin \phi)^2 \gamma_1 + \tau_0 \quad (4.36)$$

where ρ, γ_1, V and ϕ are the density of the workpiece, plastic shear strain at the exit, cutting speed and the shear angle, consecutively.

4.3.3.2. Secondary Deformation Zone

For the modelling of the secondary zone, two-zone contact model is used [3]. According to the two-zone contact model, contact between the tool and the workpiece can be sticking or sliding. In terms of two-zone contact model, the contact edge of the tool, which has a length of l_c , is divided into two parts where l_p is the sticking zone part. For the analysis, the rake face of the tool is divided into three sections (see Figure 4.8) where the possible combinations of contact types are analysed.

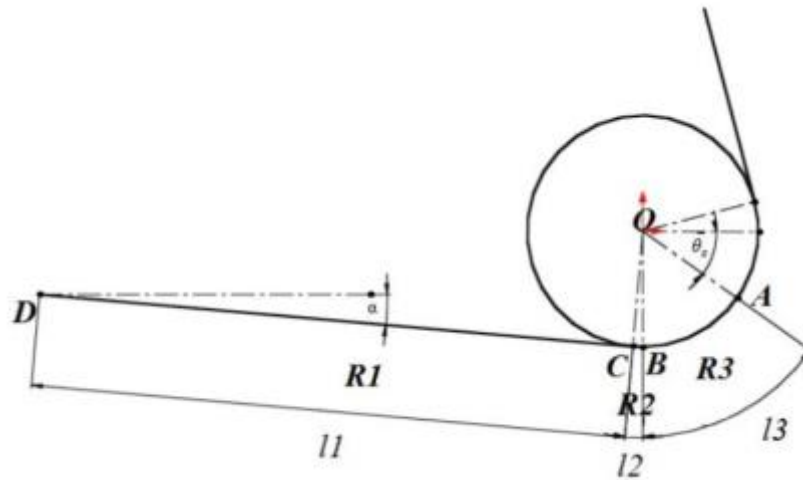


Figure 4.8 - Regions on the rake face of the tool

The separation of the secondary and tertiary deformation zones is called stagnation point and it is marked with 'A' in Figure 4.8. The forces acting on each region in the secondary deformation zone are derived one by one.

For the first region, R1, normal force is derived as follows [94];

$$F_{N1} \begin{pmatrix} F_{N1x} \\ F_{N1y} \end{pmatrix} = \begin{pmatrix} \int_{l_2+l_3}^{l_c} P_0 a \left(1 - \frac{x}{l_c}\right)^\zeta \sin \alpha dx \\ \int_{l_2+l_3}^{l_c} P_0 a \left(1 - \frac{x}{l_c}\right)^\zeta \cos \alpha dx \end{pmatrix} \quad (4.37)$$

where x is the distance from the tool tip, a is the depth of cut, ζ is the distribution expo, l_c is the contact length and the l_p is the sticking zone. Lengths of the regions can be calculated as follows;

$$l_3 = r \left(\frac{\pi}{2} - \theta_s \right) \quad (4.38)$$

$$l_2 = r\alpha \quad (4.39)$$

$$l_c = l_1 + l_2 + l_3 \quad (4.40)$$

For R1, the friction can be either only sliding or the combination of sliding and sticking. If the sticking zone length, l_p is larger than $l_2 + l_3$, it means that the sticking zone exist in R1. However, if it is smaller than $l_2 + l_3$, sticking zone ends within the boundaries of R2, and there is only sliding friction force in R1. The calculations for both cases are shown below [94];

$$F_{F1} \begin{pmatrix} F_{F1x} \\ F_{F1y} \end{pmatrix} = \begin{cases} \begin{pmatrix} - \int_{l_2+l_3}^{l_c} \mu P_0 \left(1 - \frac{x}{l_c}\right)^\zeta \cos \alpha dx, \\ \int_{l_2+l_3}^{l_c} \mu P_0 \left(1 - \frac{x}{l_c}\right)^\zeta \sin \alpha dx \end{pmatrix}, & l_p \leq l_2 + l_3 \\ \begin{pmatrix} - \int_{l_2+l_3}^{l_p} \tau_1 w dx + \int_{l_p}^{l_c} \mu P_0 \left(1 - \frac{x}{l_c}\right)^\zeta \cos \alpha dx \\ \int_{l_2+l_3}^{l_p} \tau_1 w dx + \int_{l_p}^{l_c} \mu P_0 \left(1 - \frac{x}{l_c}\right)^\zeta \sin \alpha dx \end{pmatrix}, & l_p > l_2 + l_3 \end{cases} \quad (4.41)$$

For the second region, R2, normal force is derived as follows [94];

$$F_{N2} \begin{pmatrix} F_{N2x} \\ F_{N2y} \end{pmatrix} = \begin{cases} \int_{l_3}^{l_2+l_3} P_0 W \left(1 - \frac{x}{l_c}\right)^\zeta \sin \left(\frac{x}{r} - \frac{\pi}{2} + \theta_s \right) dx \\ \int_{l_3}^{l_2+l_3} P_0 W \left(1 - \frac{x}{l_c}\right)^\zeta \cos \left(\frac{x}{r} - \frac{\pi}{2} + \theta_s \right) dx \end{cases} \quad (4.42)$$

The friction force formulation depends on three cases for R2. Friction on R2 could be only sliding, combination of sliding and sticking, or only sticking. The cases are listed below sequentially [94];

$$F_{F2} \begin{pmatrix} F_{F2x} \\ F_{F2y} \end{pmatrix} = \begin{cases} \begin{pmatrix} -\int_{l_3}^{l_2+l_3} \mu P_0 \left(1 - \frac{x}{l_c}\right)^\zeta \cos\left(\frac{x}{r} - \frac{\pi}{2} + \theta_s\right) dx, \\ \int_{l_3}^{l_2+l_3} \mu P_0 \left(1 - \frac{x}{l_c}\right)^\zeta \sin\left(\frac{x}{r} - \frac{\pi}{2} + \theta_s\right) dx \end{pmatrix}, & l_p \leq l_3 \\ \begin{pmatrix} -\int_{l_3}^{l_p} \tau_1 w \cos\left(\frac{x}{r} - \frac{\pi}{2} + \theta_s\right) dx - \int_{l_p}^{l_2+l_3} \mu P_0 \left(1 - \frac{x}{l_c}\right)^\zeta \cos\left(\frac{x}{r} - \frac{\pi}{2} + \theta_s\right) dx \\ \int_{l_3}^{l_p} \tau_1 w \sin\left(\frac{x}{r} - \frac{\pi}{2} + \theta_s\right) dx + \int_{l_p}^{l_2+l_3} \mu P_0 \left(1 - \frac{x}{l_c}\right)^\zeta \sin\left(\frac{x}{r} - \frac{\pi}{2} + \theta_s\right) dx \end{pmatrix}, & l_2 + l_3 > l_p > l_3 \\ \begin{pmatrix} -\int_{l_3}^{l_2+l_3} \tau_1 w \cos\left(\frac{x}{r} - \frac{\pi}{2} + \theta_s\right) dx \\ \int_{l_3}^{l_2+l_3} \tau_1 w \sin\left(\frac{x}{r} - \frac{\pi}{2} + \theta_s\right) dx \end{pmatrix}, & l_p \geq l_2 + l_3 \end{cases} \quad (4.43)$$

For the third region, R2, normal force is derived as follows [94];

$$F_{N3} \begin{pmatrix} F_{N3x} \\ F_{N3y} \end{pmatrix} = \begin{cases} -\int_0^{l_3} P_0 w \left(1 - \frac{x}{l_c}\right)^\zeta \cos\left(\frac{x}{r} + \theta_s\right) dx \\ \int_0^{l_3} P_0 w \left(1 - \frac{x}{l_c}\right)^\zeta \sin\left(\frac{x}{r} + \theta_s\right) dx \end{cases} \quad (4.44)$$

The friction force acting on R3 could be combinations of sliding and sticking zones, or only sticking friction may exist. The cases are given below sequentially [94];

$$F_{F3} \begin{pmatrix} F_{F3x} \\ F_{F3y} \end{pmatrix} = \begin{cases} \begin{pmatrix} -\int_0^{l_p} \tau_1 w \sin\left(\frac{x}{r} + \theta_s\right) dx - \int_{l_p}^{l_3} \mu P_0 \left(1 - \frac{x}{l_c}\right)^\zeta \sin\left(\frac{x}{r} + \theta_s\right) dx, \\ -\int_0^{l_p} \tau_1 w \cos\left(\frac{x}{r} + \theta_s\right) dx - \int_{l_p}^{l_3} \mu P_0 \left(1 - \frac{x}{l_c}\right)^\zeta \cos\left(\frac{x}{r} + \theta_s\right) dx \end{pmatrix}, & l_p < l_3 \\ \begin{pmatrix} -\int_0^{l_p} \tau_1 w \sin\left(\frac{x}{r} + \theta_s\right) dx \\ -\int_0^{l_p} \tau_1 w \cos\left(\frac{x}{r} + \theta_s\right) dx \end{pmatrix}, & l_p \geq l_3 \end{cases} \quad (4.45)$$

For the oblique cutting approach, several changes are made on the formulations [94]. First of all, the shear stress at the exit is calculated with considering the effect of the helix angle, λ_s as [94];

$$\tau_1 = \rho(V \sin \emptyset \cos \lambda_s)^2 \gamma_1 + \tau_0 \quad (4.46)$$

The normal forces can be found by;

$$F_{Ni} = \int_i^{i+1} P_o w_c \left(1 - \frac{x}{l_c}\right)^\zeta dx \quad (4.47)$$

$$P_0 = \tau_1 \frac{h_1(\zeta+1)}{l_c \sin \emptyset} \frac{\cos \lambda \cos \eta_s}{\cos(\emptyset+\lambda-\alpha) \cos \eta_c} \quad (4.48)$$

$$w_c = \frac{\cos \eta_c}{\cos i} \quad (4.49)$$

The total contact length on the rake face, l_c can be calculated from [94];

$$l_c = h_1 \frac{(\zeta+2)}{2} \frac{\sin(\emptyset+\lambda-\alpha)}{\sin \emptyset \cos \lambda \cos \eta_c} \quad (4.50)$$

where w_c is the oblique cutting depth, i is the helix angle and η_c is the chip flow angle which can be calculated from [94];

$$(A_1^2 + B_1^2)(\sin \eta_c)^4 - (2A_1C)(\sin \eta_c)^3 + 2(A_1C + CD) \sin \eta_c + (C^2 - B_1^2 - 2A_1^2 - 2A_1D)(\sin \eta_c)^2 + (A_1^2 + D^2 + 2A_1D) = 0 \quad (4.51)$$

for which, the necessary unknowns can be found by the following equations [94];

$$A_1 = -\tan i (\tan \emptyset \sin \alpha + \cos \alpha) \quad (4.52)$$

$$B_1 = \tan \emptyset \quad (4.53)$$

$$C = \tan \lambda_a \quad (4.54)$$

$$D = \tan i \tan \beta (\cos \alpha \tan \emptyset - \sin \emptyset) \quad (4.55)$$

Shear stress and shear flow angle are calculated as [94];

$$F_s = \tau_1 \frac{wh_1}{\sin \emptyset \cos i} \quad (4.56)$$

$$\eta_s = \tan^{-1} \left(\frac{\tan i \cos(\emptyset-\alpha) - \tan \eta_c \sin \emptyset}{\cos \alpha} \right) \quad (4.57)$$

4.3.3.3. Third Deformation Zone

The forces in the third deformation zone are consequences of the contact between the tool and the newly formed surface due to ploughing. As mentioned previously, the stagnation point, A separated the secondary and third deformation zones. The third deformation zone is the following region from A to the follow-up region on the flank edge of the tool as seen in Figure 4.7.

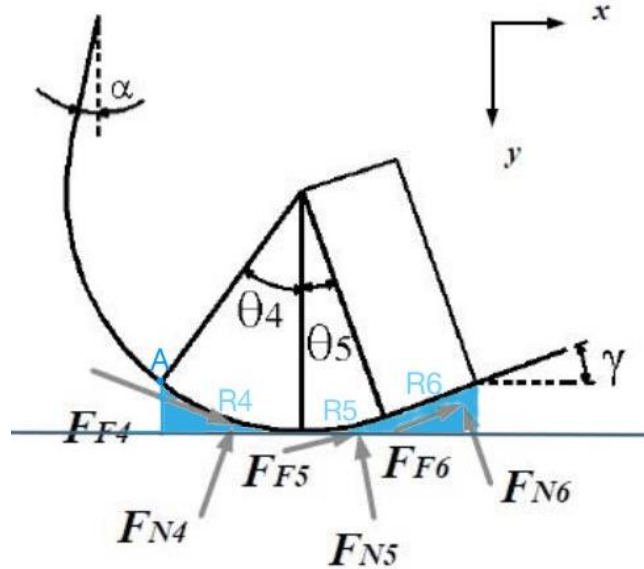


Figure 4.9 – Third deformation zone regions and ploughing depth

Just as in the secondary deformation zone, third deformation zone is also divided into three regions which are going to be referred as R4, R5 and R6 (see Figure 4.9). Contact lengths for each is given below [4];

$$l_4 = r\theta_s \quad (4.58)$$

$$l_5 = r\gamma \quad (4.59)$$

$$l_{c_thirdzone} = l_4 + l_5 + l_6 \quad (4.60)$$

In the third deformation zone, the normal pressure is found to be related with the ploughing depth, which is shown as blue shaded area in Figure 4.9. The formulation for the normal pressure in third deformation zone is suggested as follows;

$$P3(x) = ax^2 + bx + c \quad (4.61)$$

where x is the distance from the tool tip and;

$$a = \frac{((P_0 l_{c_thirdzone}) - P_0 (P_{MAX} l_{c_thirdzone}))}{(l_{c_thirdzone}^2 - (l_c l_4))} \quad (4.62)$$

$$b = \frac{P_{MAX}}{l_4} - (a l_4) - \left(\frac{P_0}{l_4}\right) \quad (4.63)$$

$$c = P_0 \quad (4.64)$$

For the fourth region, R4, normal force is derived as follows [3];

$$F_{N4} \begin{pmatrix} F_{N4x} \\ F_{N4y} \end{pmatrix} = \begin{pmatrix} \int_0^{l_4} w P3(x) \cos\left(\frac{\pi}{2} + \frac{x}{r} - \theta_s\right) dx \\ - \int_0^{l_4} w P3(x) \sin\left(\frac{\pi}{2} + \frac{x}{r} - \theta_s\right) dx \end{pmatrix} \quad (4.65)$$

P_{MAX} is modelled experimentally as [3];

$$P_{MAX} = P_0(-0.013r_c + 1.891) \quad (4.66)$$

where w is the axial depth of cut. For the friction forces, there are three possible cases. The first one is the case when the sticking contact length, l_p is 0. In this case, only sliding friction exists. In the second case, l_p is smaller than l_4 , so R4 has both sliding and sticking regions. The last case exists when l_p is larger than l_4 which leads to only sticking friction in R4. All cases are given below sequentially as mentioned [3];

$$F_{F4} \begin{pmatrix} F_{F4x} \\ F_{F4y} \end{pmatrix} = \begin{cases} \begin{pmatrix} \int_0^{l_4} \mu P3(x) \sin\left(\frac{\pi}{2} + \frac{x}{r} - \theta_s\right) dx \\ \int_0^{l_4} \mu P3(x) \cos\left(\frac{\pi}{2} + \frac{x}{r} - \theta_s\right) dx \end{pmatrix}, & l_p = 0 \\ \begin{pmatrix} \int_0^{l_p.thirdzone} \tau_1 w \sin\left(\frac{x}{r} - \frac{\pi}{2} + \theta_s\right) dx + \int_{l_p.thirdzone}^{l_4} \mu P3(x) \sin\left(\frac{\pi}{2} + \frac{x}{r} - \theta_s\right) dx \\ \int_0^{l_p.thirdzone} \tau_1 w \cos\left(\frac{\pi}{2} + \frac{x}{r} - \theta_s\right) dx + \int_{l_p.thirdzone}^{l_4} \mu P3(x) \cos\left(\frac{\pi}{2} + \frac{x}{r} - \theta_s\right) dx \end{pmatrix}, & 0 > l_p > l_4 \\ \begin{pmatrix} \int_0^{l_4} \tau_1 w \sin\left(\frac{\pi}{2} + \frac{x}{r} - \theta_s\right) dx \\ \int_0^{l_4} \tau_1 w \cos\left(\frac{\pi}{2} + \frac{x}{r} - \theta_s\right) dx \end{pmatrix}, & l_p \geq l_4 \end{cases} \quad (4.67)$$

For the fifth region, R5, normal force is derived as follows [3];

$$F_{N5} \begin{pmatrix} F_{N5x} \\ F_{N5y} \end{pmatrix} = \begin{pmatrix} - \int_{l_4}^{l_4+l_5} w P3(x) \sin\left(\frac{x}{r} - \theta_s\right) dx \\ - \int_{l_4}^{l_4+l_5} w P3(x) \cos\left(\frac{x}{r} - \theta_s\right) dx \end{pmatrix} \quad (4.68)$$

Again, there are three possible cases for the friction forces in R5. The first one is the case when the sticking contact length, l_p is less than l_4 . In this case, only sliding friction exists. In the second case, l_p is in between l_4 and $l_4 + l_5$, so R5 has both sliding and sticking regions. The last case exists when l_p is larger than l_5 which leads to only sticking friction in R5. All cases are given below sequentially as mentioned [3];

$$F_{F5} \begin{pmatrix} F_{F5x} \\ F_{F5y} \end{pmatrix} = \begin{cases} \begin{pmatrix} \int_{l_4}^{l_4+l_5} \mu P3(x) \cos\left(\frac{x}{r} - \theta_s\right) dx \\ \int_{l_4}^{l_4+l_5} \mu P3(x) \sin\left(\frac{x}{r} - \theta_s\right) dx \end{pmatrix}, & l_p < l_4 \\ \begin{pmatrix} \int_{l_4}^{l_p.thirdzone} \tau_1 w \cos\left(\frac{x}{r} - \theta_s\right) dx + \int_{l_p.thirdzone}^{l_4+l_5} \mu P3(x) \cos\left(\frac{x}{r} - \theta_s\right) dx \\ - \int_{l_4}^{l_p.thirdzone} \tau_1 w \sin\left(\frac{x}{r} - \theta_s\right) dx - \int_{l_p.thirdzone}^{l_4+l_5} \mu P3(x) \sin\left(\frac{x}{r} - \theta_s\right) dx \end{pmatrix}, & l_4 < l_p < l_4 + l_5 \\ \begin{pmatrix} \int_{l_4}^{l_4+l_5} \tau_1 w \cos\left(\frac{x}{r} - \theta_s\right) dx \\ - \int_{l_4}^{l_4+l_5} \tau_1 w \sin\left(\frac{x}{r} - \theta_s\right) dx \end{pmatrix}, & l_p \geq l_4 \end{cases} \quad (4.69)$$

For the last region on the flank face, R6, normal force is derived as follows [3];

$$F_{N6} \begin{pmatrix} F_{N6x} \\ F_{N6y} \end{pmatrix} = \begin{pmatrix} - \int_{l_4+l_5}^{l_c.thirdzone} w P3(x) \sin(\gamma) dx \\ - \int_{l_4+l_5}^{l_c.thirdzone} w P3(x) \cos(\gamma) dx \end{pmatrix} \quad (4.70)$$

Friction forces in R5 may appear in three cases as well. The first one is the case when the sticking contact length, l_p is less than $l_4 + l_5$. In this case, only sliding friction exists in R6. In the second case, l_p is in between $l_4 + l_5$ and l_6 , so R6 has both sliding and sticking regions. The last case exists when l_p is larger than l_6 which leads only sticking friction to appear in R6. All cases are given below sequentially as mentioned [3];

$$F_{F6} \begin{pmatrix} F_{F6x} \\ F_{F6y} \end{pmatrix} = \begin{cases} \begin{pmatrix} \int_{l_4+l_5}^{l_{c_thirdzone}} \mu P3(x) \cos(\gamma) dx \\ - \int_{l_4+l_5}^{l_{c_thirdzone}} \mu P3(x) \sin(\gamma) dx \end{pmatrix}, & l_p < l_4 + l_5 \\ \begin{pmatrix} \int_{l_4+l_5}^{l_{p_thirdzone}} \tau_1 w \cos(\gamma) dx + \int_{l_{p_thirdzone}}^{l_{c_thirdzone}} \mu P3(x) \cos(\gamma) dx \\ - \int_{l_4+l_5}^{l_{p_thirdzone}} \tau_1 w \sin(\frac{x}{r} - \theta_s) dx - \int_{l_{p_thirdzone}}^{l_{c_thirdzone}} \mu P3(x) \sin(\gamma) dx \end{pmatrix}, & l_4 + l_5 < l_p < l_6 \\ \begin{pmatrix} \int_{l_4+l_5}^{l_{c_thirdzone}} \tau_1 w \cos(\gamma) dx \\ - \int_{l_4+l_5}^{l_{c_thirdzone}} \tau_1 w \sin(\gamma) dx \end{pmatrix}, & l_p = l_{c_thirdzone} \end{cases} \quad (4.71)$$

Forces acting on the tool have two common directions; direction of feed and tangential direction, where F_f and F_t are the total forces exerted in the feed and tangential direction sequentially, F_{fc} and F_{tc} are the cutting forces in these directions, and F_{fe} and F_{te} are the edge forces in these directions;

$$F_f = F_{fc} + F_{fe} \quad (4.72)$$

$$F_t = F_{tc} + F_{te} \quad (4.73)$$

There are also bottom edge forces which are caused by the contact between the tool tip and the workpiece. These forces and cutting coefficients can be found experimentally [3]. Total forces acting on the tool can be found by summing up feed and tangential forces acting in all deformation zones;

$$F_{Feed} = F_{F_{Primary}} + F_{F_{Secondary}} + F_{F_{Third}} + F_{F_{Bottom}} \quad (4.74)$$

$$F_{Tangential} = F_{T_{Primary}} + F_{T_{Secondary}} + F_{T_{Third}} + F_{T_{Bottom}} \quad (4.75)$$

4.4 Optimization of Micromilling Process

MATLAB code is developed for micromilling process optimization regarding the objective functions and constraints explained in previous sections. Decision variables are chosen to be cutting speed, V_c , feed rate, f , and axial depth of cut, d for both roughing and finishing operations. Before the initiation, upper and lower bound values for decision variables are given to determine the range of values that the code will output. For depth of cut, total stock to be removed is also entered. In order to avoid ploughing mechanism, minimum chip thickness is calculated as 20-40% of hone radius [25]. The lower bound of depth of cut for each pass is set respecting minimum chip thickness after hone radii measurements under microscope. Code also calculates the optimum number of roughing passes respecting the upper bound of depth of cut given. As an output, code generates a matrix of solution set including the number of roughing passes, and V_c , f , d values for each roughing pass and finishing pass.

Some parameters for MOPSO algorithm is determined in the next step. These parameters are the maximum number of iterations, which is the stopping criteria, number of the population size and repository size, inertia weight and its damping rate, and learning coefficients as in Figure 4.10. These constant values are commonly used values in literature. For the maximum iteration number, it is observed that the Pareto curve does not change after 100 iterations roughly. Figure 4.11 shows Pareto curves from different runs with maximum iteration number is set to 100, 150 and 200 consequently. Particles converge towards the global bests as iteration number increases. It is clear that no change occurs in Pareto curve after 100 iterations roughly. Therefore, maximum number of iterations is set to 150 for safety.

```
%% MOPSO Parameters

MaxIt=150;           % Maximum Number of Iterations

nPop=200;           % Population Size

nRep=100;           % Repository Size

w=0.5;              % Inertia Weight
wdamp=0.99;         % Intertia Weight Damping Rate
c1=1;               % Personal Learning Coefficient
c2=2;               % Global Learning Coefficient
```

Figure 4.10 - MOPSO parameters

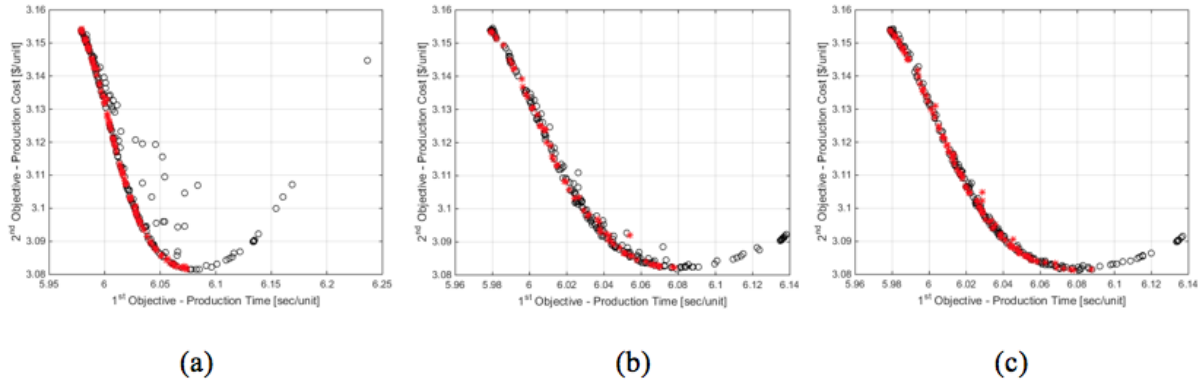


Figure 4.11 - (a) Max. iteration = 100; (b) Max. iteration = 150; (c) Max. iteration = 200

In the initiation part of the code, initial positions and velocities of each particle are randomized. Values of objective functions for each particle are calculated and those values are accepted as the personal best values for the initiation. These values are stored in the external archive.

For a better selection of global best, better convergence of solutions is needed. For this purpose, neighbouring topology is used as in the study of Coello Coello et al. [88]. In their study, an external repository is created in order to store nondominated solutions found so far. The external repository consists of two parts. The first one is the ‘Archive Controller’. The function of the archive controller is to control storing the new element to the archive or not by checking the dominance of the new element over the previous particles added to the archive. When the archive reaches to its maximum capacity, second part of the repository is triggered which is the ‘Adaptive Grid’. Adaptive grid creates hypercubes, which are a type of neighbourhood, containing a certain number of particles. The particles are grouped into neighbourhoods uniformly. Grid sizes can be defined by the user. Each hypercube is given a fitness value considering the number of particles inside it. Roulette Wheel approach is used to select a hypercube depending on its assigned fitness value. One hypercube is selected and a global leader is randomly selected inside that hypercube. The adaptive grid and roulette wheel approach encourages particles to be selected from the least crowded hypercubes which provides diversity and prevents premature convergence.

As non-dominating Pareto solutions are selected and stored in an external repository, main loop of the algorithm selects leaders updates each particle’s velocities and positions towards the leaders.

Mutation operator is another method to overcome premature convergence. As mentioned in the previous sections, in some cases, velocity of particles converges to 0 and code fails to generate new solutions and diversity is lost. For those particles trapped in a local optimum, mutation operator is used. A single particle is mutated with a randomized velocity or position, in order to escape from local convergence. As the number of iterations increase, the effect of mutation operator decreases. If the personal best of each particle is dominated by its new position, its personal best is updated. The archive is updated with the global best values in each iteration. Pseudo-code of generated MATLAB code can be summarized as in Figure 4.12 and the code generates a Pareto curve for two objective function values as in **Error! Reference source not found.**

```

begin

    for each particle of the swarm
        Initialize random position
        Initialize random velocity
        Compute fitness values
        Update personal best values with initial positions
    end for

    Initialize an external archive with non-dominated solutions

    while maximum iteration number is not reached
        for each particle of the swarm
            Select a leader from the repository
            Update velocity vectors
            Update position
            Apply mutation operator
            Compute fitness values
            Update personal bests
        end for
        Update external archive with non-dominated solutions
    end

    plot objective function values

end begin

```

Figure 4.12 - Pseudo-code of MOPSO

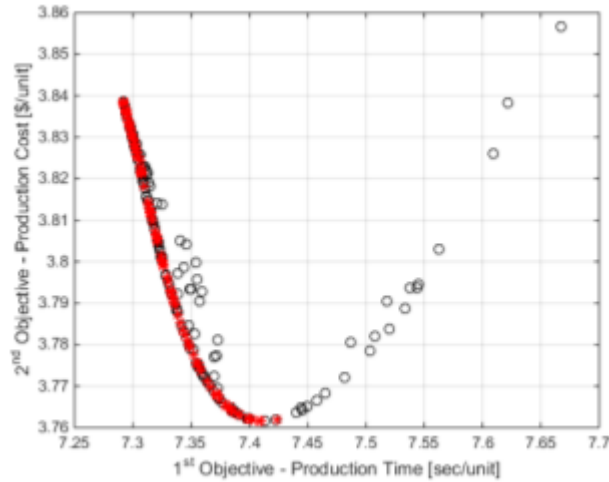


Figure 4.13 - Pareto curve generated by MATLAB code

4.5 Summary

In this section, models and formulations which are going to be used in MOPSO algorithm are presented. The objective functions are selected as the production time and cost. They have a contradicted relation. In order to decrease production time, cutting speed could be increased, which on the other hand may decrease tool life, so the production cost increases. MATLAB code generated Pareto curve representing the relation of production time and cost. Meanwhile, surface roughness, burr size and cutting forces have limitation values. So the generated process parameters should result in process performances respecting these limitations. Decision variables which the code would generate is the number of roughing passes, and cutting speed, feed rate and the depth of cut for roughing and finishing passes.

5. APPLICATIONS AND CASE STUDIES

5.1 Verification Test Setup

In this section, results of verification tests for MATLAB code is presented. As mentioned in the previous section, MATLAB code generates V_c , f , and d values for each roughing pass and the finishing pass. Two sets of cutting tests are applied. First, regular slotting tests are done with commonly used cutting parameters regarding the specified cutting tool and the workpiece. The values are average values taken from tests in literature and suggested values on tool catalogue. Parameter values used in the first set of tests are listed in Table 5.1.

The second set of tests are conducted with the cutting parameters obtained from MATLAB code. Since the code generates cutting parameters for the finishing pass, there are values for finishing operation as well in Table 5.2. Surface roughness, burr formation and cutting forces are also measured for each slot in order to observe optimization results. Table 5.1 and Table 5.2 only includes values for production time, cutting force and surface roughness measurements. Additional tests are conducted for tool wear measurement. Tool wear is investigated under microscope to observe changes in tool life with optimized cutting parameters which would lead to lower production costs.

Table 5.1 –First set of tests with recommended cutting parameters

Test No	Target Axial DoC (mm)	Number of Teeth	ROUGHING				
			Feed per Tooth, fz (mm)	Feed, f (mm/min)	Spindle Speed, n (rpm)	Cutting Speed, Vc (m/min)	Axial DoC, d (mm)
1	0,1	4	0,002	80	10000	62,80	0,02
2	0,1	4	0,006	240	10000	62,80	0,02
3	0,1	4	0,01	400	10000	62,80	0,02
4	0,1	4	0,002	80	10000	62,80	0,05
5	0,1	4	0,006	240	10000	62,80	0,05
6	0,1	4	0,01	400	10000	62,80	0,05
7	0,1	4	0,002	120	15000	94,20	0,02
8	0,1	4	0,006	360	15000	94,20	0,02
9	0,1	4	0,01	600	15000	94,20	0,02
10	0,1	4	0,002	120	15000	94,20	0,05
11	0,1	4	0,006	360	15000	94,20	0,05
12	0,1	4	0,01	600	15000	94,20	0,05

Table 5.2 – Second set of tests with code generated cutting parameters

Run No	Target Axial DoC (mm)	Number of Teeth	ROUGHING					FINISHING				
			Feed per Tooth, fz (mm)	Feed, f (mm/min)	Spindle Speed, n (rpm)	Cutting Speed, Vc (m/min)	Axial DoC, d (mm)	Feed per Tooth, fz (mm)	Feed, f (mm/min)	Spindle Speed, n (rpm)	Cutting Speed, Vc (m/min)	Axial DoC, d (mm)
1	0,1	4	0,00660273	420,64	15926,7516	100,02	0,05	0,00484924	303	15621,0191	98,10	0,01
2	0,1	4	0,0066455	422,73	15902,8662	99,87	0,05	0,0047918	305,21	15923,5669	100,00	0,01
3	0,1	4	0,00772061	512,56	16597,1338	104,23	0,08	0,00260846	220,24	21108,2803	132,56	0,02
4	0,1	4	0,00842698	560,26	16621,0191	104,38	0,08	0,00280859	220	19582,8025	122,98	0,02
5	0,1	4	0,0053885	360	16702,2293	104,89	0,04	0,00151789	120	19764,3312	124,12	0,02
6	0,1	4	0,0087381	539,87	15445,8599	97,00	0,09	0,00232011	176,89	19060,5096	119,70	0,01
7	0,1	4	0,00857096	532	15517,5159	97,45	0,09	0,00230794	154	16681,5287	104,76	0,01
8	0,1	4	0,00566048	360,54	15923,5669	100,00	0,04	0,00240923	194,58	20191,0828	126,80	0,02
9	0,1	4	0,01171756	612	13057,3248	82,00	0,07	0,00204751	147,89	18057,3248	113,40	0,03
10	0,1	4	0,00866936	582,89	16808,9172	105,56	0,07	0,00472468	308,97	16348,7261	102,67	0,03
11	0,1	4	0,00915353	603,2	16474,5223	103,46	0,08	0,00451502	289,45	16027,0701	100,65	0,02
12	0,1	4	0,00601129	480,98	20003,1847	125,62	0,08	0,00389226	303,2	19474,5223	122,30	0,02

In both sets of tests, slot milling is conducted with micro end mills with 2 mm in diameter and 4 flutes on Ti-6Al-4V titanium alloy workpiece with cutting parameters listed in in Table 5.1 and Table 5.2. Each slot is 15 mm in length and total depth of cut is 0.1 mm. The workpiece is prepared before in 65x65 mm dimensions and milled on KERN Evo Ultra Precision CNC Machining Centre with the resolution of 0.1 μm and positioning tolerance of $\pm 0.1 \mu\text{m}$ shown in Figure 5.2. Cutting forces are measured with Kistler type 9256C dynamometer in Figure 5.2. Tool wear, surface roughness and burr size are examined under Nanofocus μsurf Explorer in Figure 5.2.

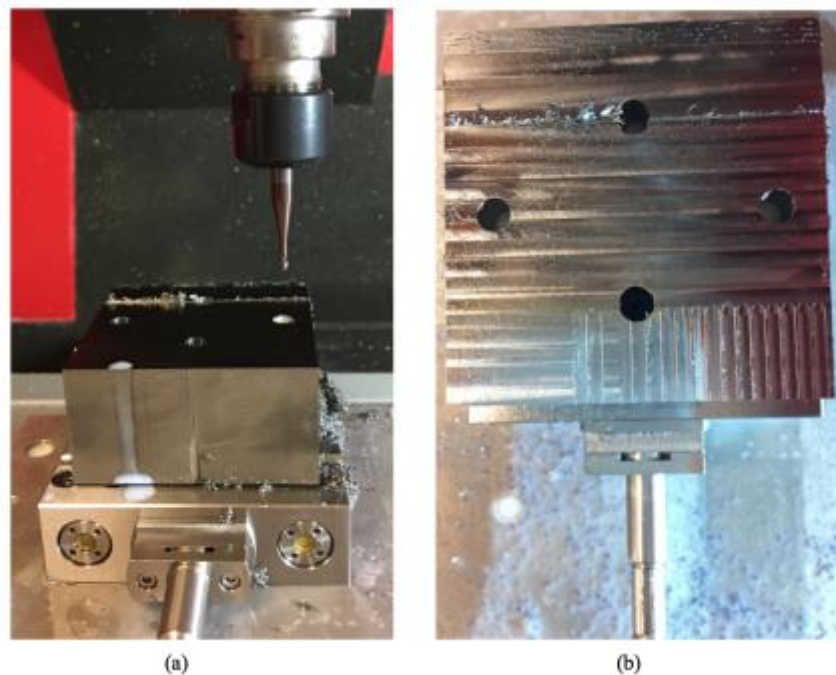


Figure 5.1 – (a) Tool and Workpiece Setup, (b) Slot Milling Operation



Figure 5.2 – (a) KERN Evo Ultra Precision Machining Centre; (b) Kistler Type 9256C; (c) Nanofocus μ surf Explorer

First, tools are observed under Nanofocus μ surf microscope and hone radii are measured as shown in Figure 5.3. It is observed that the average hone radius of the tools is $14\ \mu\text{m}$. In order to avoid ploughing mechanism, minimum chip thickness is calculated as 20-40% of hone radius [25], which makes $2.8 - 5.6\ \mu\text{m}$. The lower bound of depth of cut for each pass is set to $5.6\ \mu\text{m}$ in the code to stay on safe side.

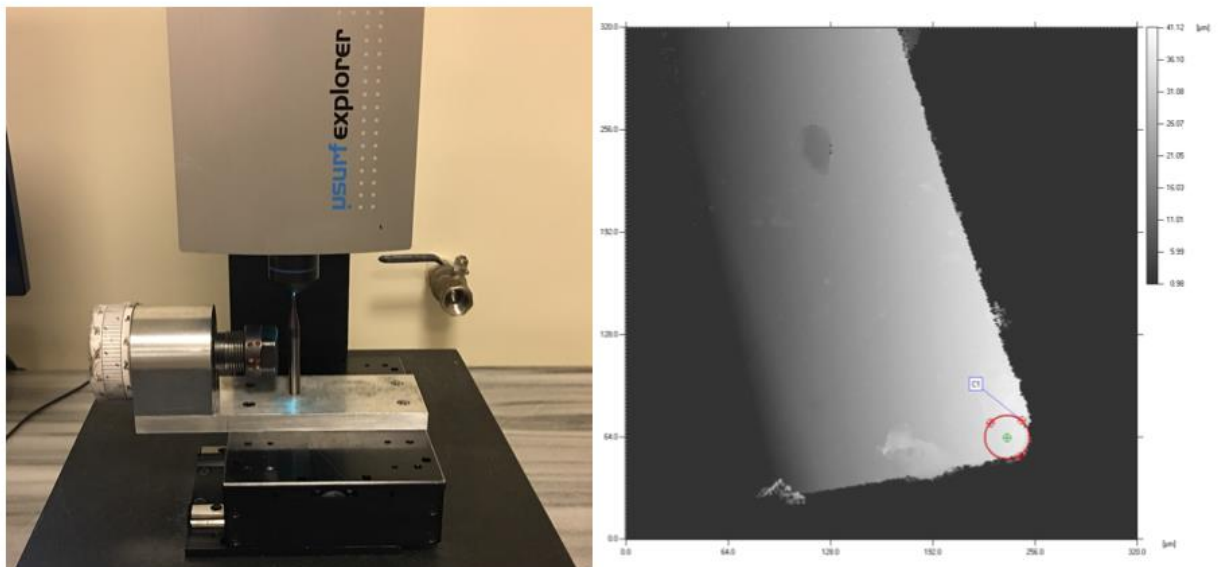


Figure 5.3 - Hone Radius Measurement under Nanofocus μ surf

In Table 5.3, measurements for cutting force components, surface roughness and production time are given from the first set of tests done with recommended cutting parameters. Table 5.4 has measurement results of tests with optimized process parameters and calculated values from the code. Results for each objective function and constraints will be explained in the following sections.

Table 5.3 - Results from recommended cutting parameters

	EXP. RESULTS			
Test No	Ff (N)	Ft (N)	Surface Roughness (μm)	Production Time (sec)
1	12,27	9,93	0,67	60,71
2	18,41	3,16	0,77	20,50
3	22,00	17,08	0,53	12,50
4	24,92	13,40	0,45	24,20
5	28,91	7,56	0,83	8,00
6	32,31	11,46	0,50	5,00
7	13,60	10,22	0,48	39,00
8	15,60	19,28	0,66	13,50
9	17,34	15,82	0,61	8,50
10	7,12	12,82	0,51	15,80
11	17,29	7,21	0,49	4,80
12	25,34	11,81	0,53	3,40

Table 5.4 - Result from optimized parameters achieved by experimental measurement and model

	EXP. RESULTS				MOD. RESULTS			
Run No	Ff (N)	Ft (N)	Surface Roughness (μm)	Production Time (sec)	Ff (N)	Ft (N)	Surface Roughness (μm)	Production Time (sec)
1	10,25	7,13	0,25	7,25	6,79	7,20	0,30	6,30
2	5,47	8,61	0,55	7,21	6,08	5,38	0,49	7,42
3	25,64	11,40	0,46	6,28	20,11	10,69	0,50	6,06
4	22,98	12,13	0,37	6,10	16,90	10,66	0,40	4,48
5	13,79	7,57	0,31	13,75	11,36	5,14	0,21	12,59
6	28,60	12,37	0,56	6,94	31,37	7,55	0,47	4,31
7	28,35	9,81	0,43	7,72	25,04	6,27	0,44	7,72
8	6,16	5,09	0,24	10,87	7,31	4,60	0,29	11,58
9	30,81	13,01	0,94	8,19	36,83	10,78	0,50	7,03
10	5,07	9,29	0,29	5,12	5,02	10,02	0,34	5,60
11	22,64	11,14	0,31	4,97	18,16	9,56	0,32	4,32
12	21,03	10,42	0,34	5,31	19,06	9,34	0,35	4,49

5.2 Results and Discussions

5.2.1 Production Time

As mentioned previously, production time is calculated as the sum of actual machining time (T_m), time wasted without cutting (T_i) and time spent during tool change (T_c). Tool changing time is a CNC machine characteristic and time spent without cutting can be reduced by feed path scheduling. Highest reduction in production time can be achieved by reducing the actual machining time, which can be done by optimizing cutting parameters by maximizing MRR.

During each slot milling, machining time is recorded in with a cutting force based chronometer. When dynamometer reads a cutting force, chronometer counts. Table 5.4 includes measured and calculated production time. Production time calculated by MATLAB code is verified with the actual measured experimental data. Below, Figure 5.4 shows that the code calculations are reliable with the error of 12.6%.

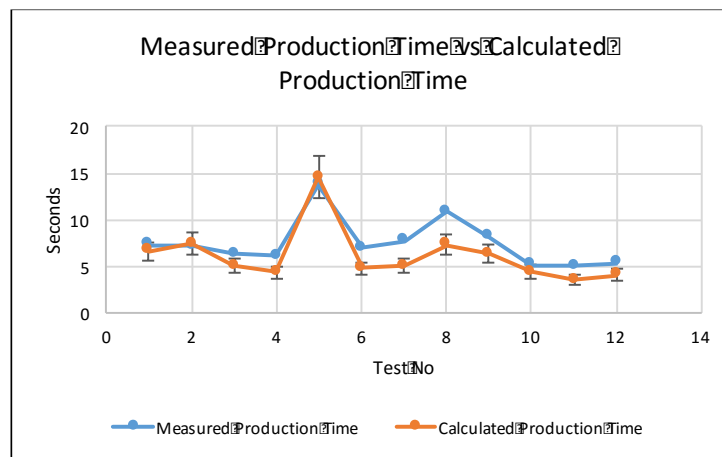


Figure 5.4 -- Measured production time vs calculated production time

In the code, each particle in the solution set favours one objective. Figure 5.5 shows one of the Pareto curves generated in different runs. As mentioned in Chapter 4, parameters minimizing the production time degrades production cost. For instance, maximizing MRR for reducing production time leads to lower tool life and increase in production cost. The Pareto curve in Figure 5.5 gives different solutions in favour of different objective functions. Peaks in Figure 5.4 belong to tests with optimized parameters favouring production cost, therefore provides longer tool life.

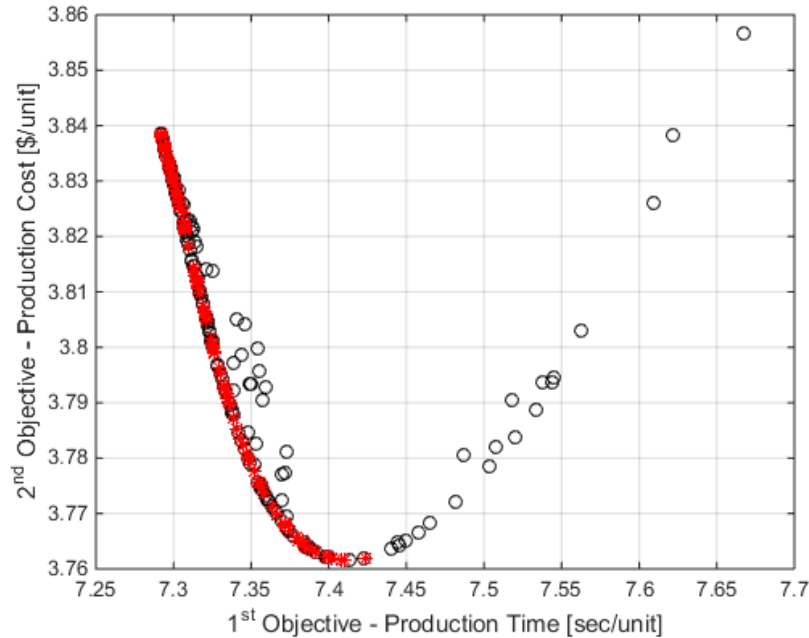


Figure 5.5 - Example of Pareto curve generated by MATLAB code

Average production time from the first set of tests and from second set of tests are shown below in Figure 5.6. As it can be seen from the graph, the average production time is reduced by %40 from the first set of tests to second one obtained by MATLAB results. Since production time is mostly effected by the actual machining time, rather than tool idling and changing time, it is possible to obtain such a big reduction by increasing MRR up to process performance and part quality limits defined. In following sections, it will be shown that production time is minimized without causing poor tool life, surface roughness or violating any other quality criteria.

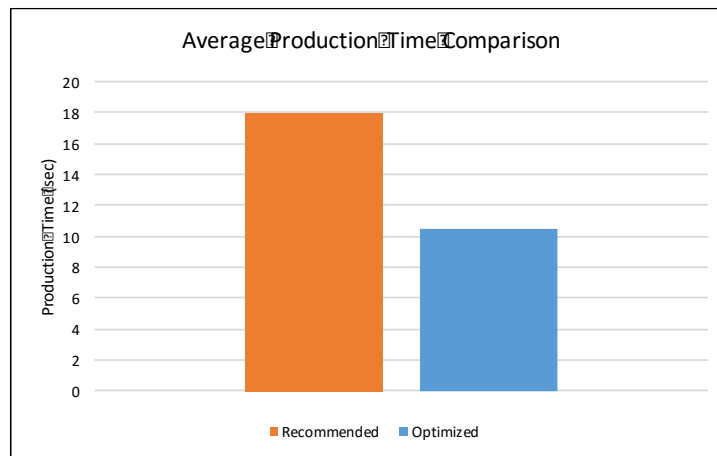


Figure 5.6 - Production time with recommended cutting parameters vs optimized cutting parameters

5.2.2 Production Cost

Total production cost includes actual machining cost, machining idle cost, cost during tool change and the tool cost. Labour and overhead costs are included in the constant, k_0 (\$ per minute). Production cost is reduced also by reducing the production time, which indirectly reduces machining costs and labour costs. The main part of reduction comes from maximized tool life. As given in Chapter 4, tool life depends on the cutting speed and constants related to tool material and geometry [11] as given in Eq. 4.12.

Hone radii of unused tools are measured under Nanofocus μ surf microscope with an objective lens of 50x. Two new tools are used at the beginning of each set of tests. Average hone radius for each tool is calculated as $14.13 \mu m$ for the first set of tests and $13.72 \mu m$ for the second set of tests. After equal number of slots are machined, hone radii are measured again and tool wear is calculated as [27];

$$Tool\ Wear = \frac{d_i + d_f}{2} \quad (5.1)$$

After cutting equal number of slots, it is seen from the measurements in Figure 5.7 that the hone radii enlarge averagely to $29.19 \mu m$ and $22.81 \mu m$ consequently. So the tool wears are calculated from Eq. 5.1 as in Figure 5.8. It is seen that tool wear rate is reduced by 21,8%.

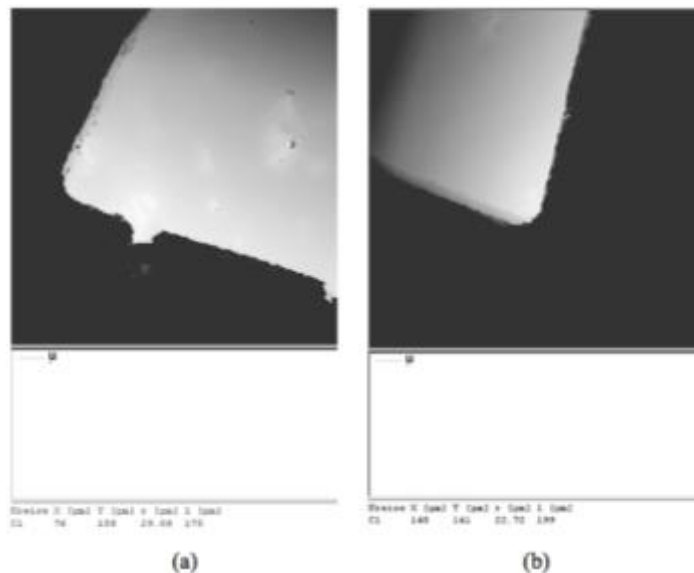


Figure 5.7 – Sample measurements of final tool hone radii; (a) with recommended parameters; (b) with optimized parameters

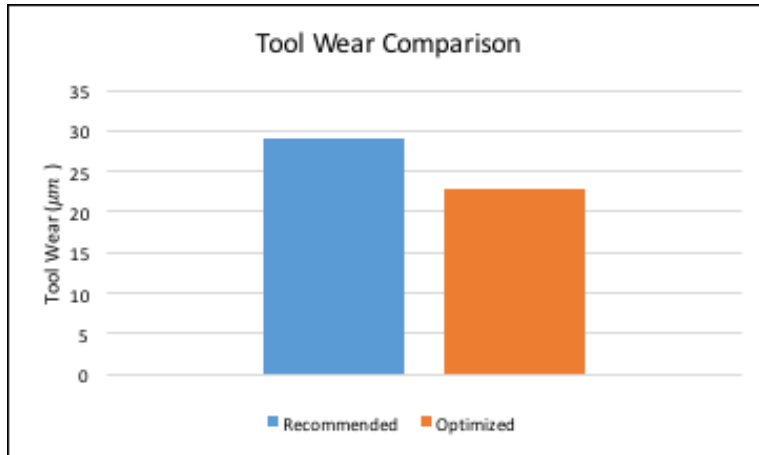


Figure 5.8 – Tool wear with recommended cutting parameters vs optimized cutting parameters

5.2.3 Surface Roughness

Surface roughness measurements are also carried out with Nanofocus µsurf microscope with an objective lens of 50x. Measured data from both sets of tests are given in the tables Table 5.3 and Table 5.4. Surface roughness values achieved by the code is verified with the test results. Figure 5.9 shows that the code calculations are reliable with an error of 15.93%. Experimental measurements show a high surface roughness value on test no 9, that is because of an unexpected chatter vibration, which is also detected from microscope image given in Figure 5.10.

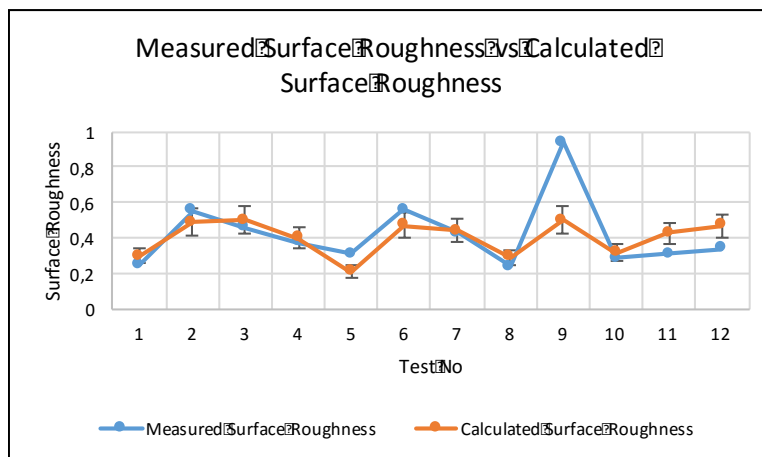


Figure 5.9 - Measured surface roughness vs calculated surface roughness

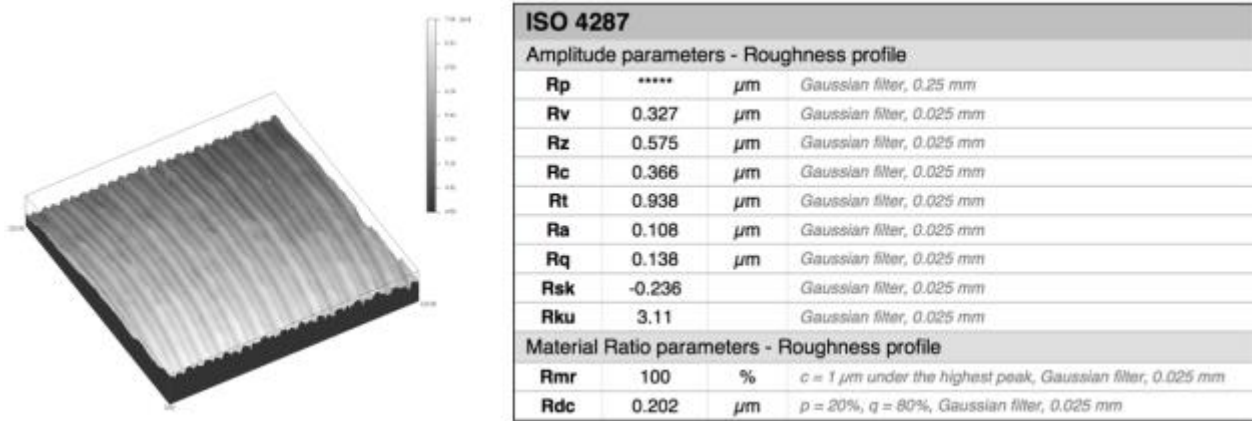


Figure 5.10 - Nanofocus image and measurement table of a chatter vibration detected

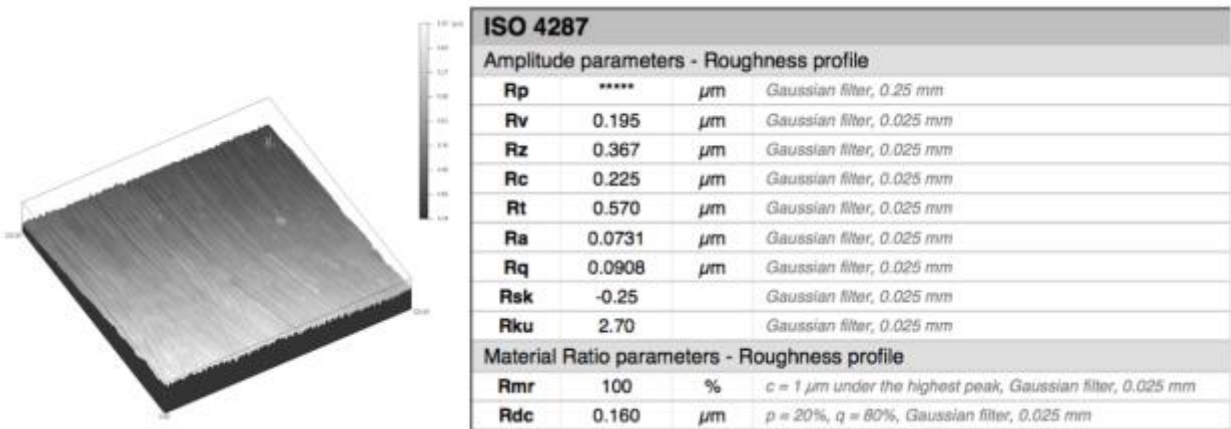


Figure 5.11 - An example measurement of surface roughness from tests with recommended cutting parameters

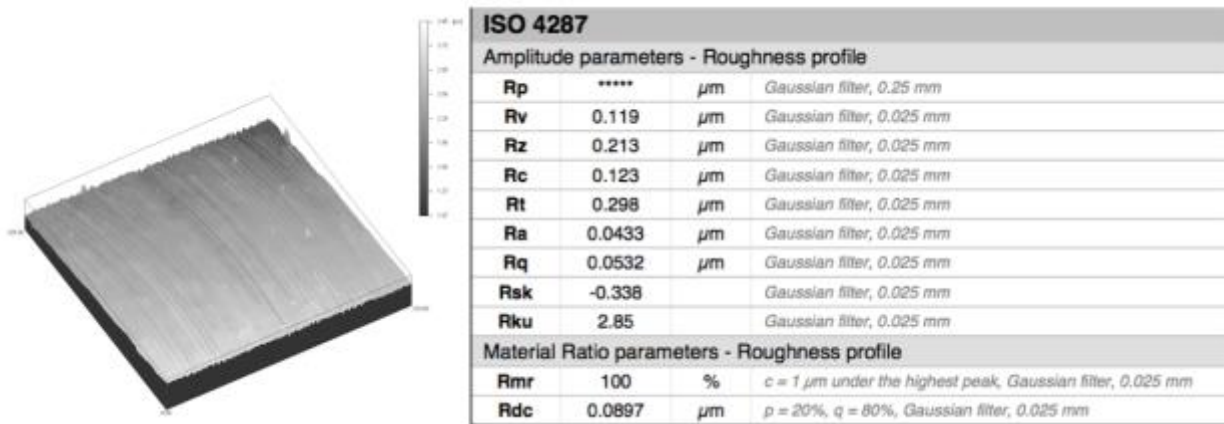


Figure 5.12 - - An example measurement of surface roughness from tests with optimized cutting parameters

After completing the first set of tests with recommended cutting parameters, surface roughness values of each slot are measured. An example from these measurements is shown in Figure 5.11. The average value of surface roughness from first set of tests is calculated as $0,58 \mu m$. Depending on the average value, the upper bound of surface roughness in the code is set to $0,5 \mu m$. Code generated values have an average surface roughness of $0,39 \mu m$. After completing the second set of tests, average surface value of experimental data is measured as $0,42 \mu m$. An example from these measurements is shown in Figure 5.12. Figure 5.3 shows the comparison of average surface roughness values from tests with recommended values and optimized values. It can be concluded that the surface roughness is decreased by 27,5% with the optimization of process parameters.

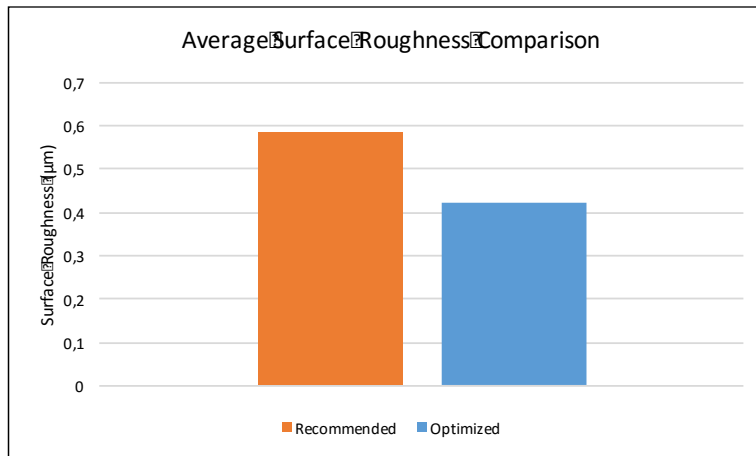


Figure 5.13 - Surface roughness with recommended cutting parameters vs optimized cutting parameters

5.2.4 Burr Formation

Burr size measurements are also carried out with Nanofocus $\mu surf$ microscope with an objective lens of 10x. A sample measurement is done, which is shown in Figure 5.14, in order to set upper bound of burr height in MATLAB code. Images taken from top clearly indicates that burr formation is kept under control as shown in Figure 5.15 and Figure 5.16.

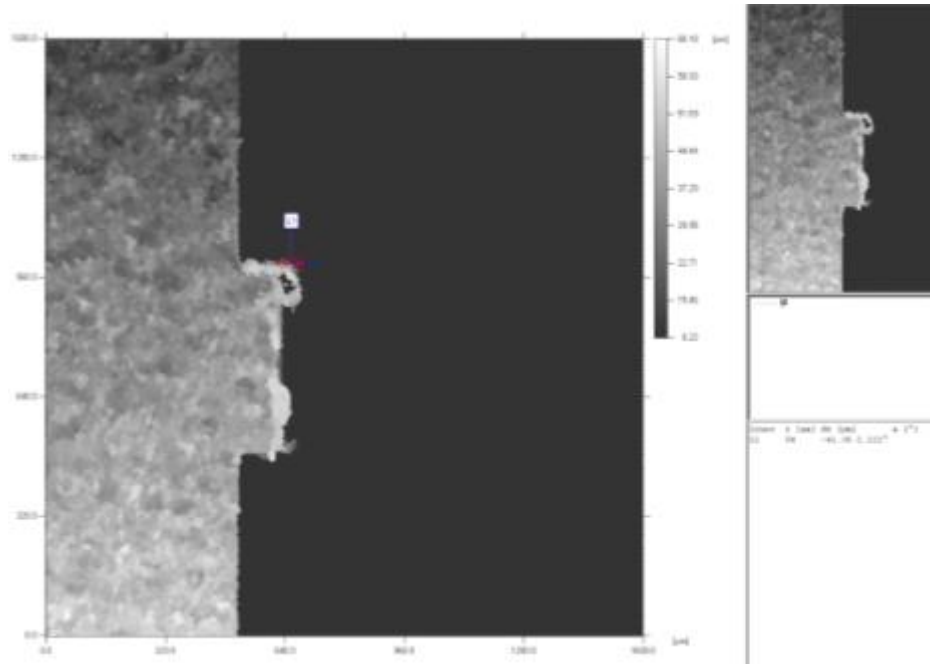


Figure 5.14 - Burr size measurement

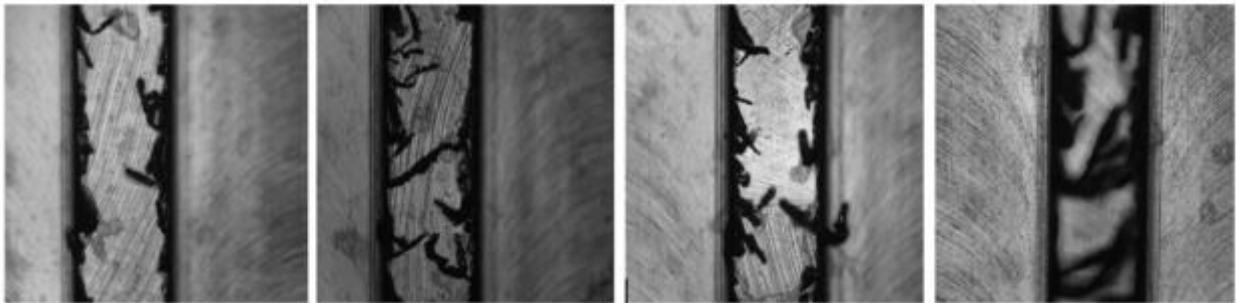


Figure 5.15 - Burr images from slots with recommended cutting parameters

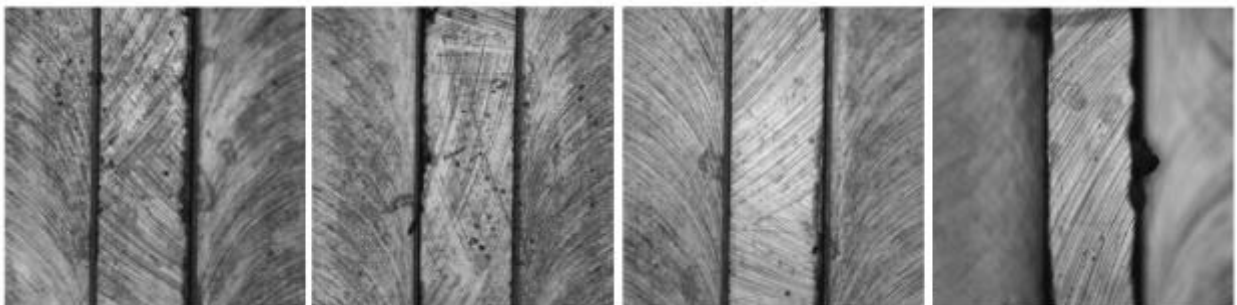


Figure 5.16 - Burr images from slots with optimized cutting parameters

5.2.5 Cutting Forces

Cutting forces are calculated according to the model mentioned in Chapter 4.3. For the primary deformation zone, Johnson Cook's parameters for Ti-6Al-4V are given in Table 5.5.

Table 5.5 - Johnson's Cook parameters for Ti-6Al-4V

A (MPa)	B (Mpa)	n	m	v
649	490	0.28	0.028	1

During the experimental tests, cutting forces are measured with Kistler type 9256C dynamometer. Measured data from both sets of tests are given in the tables Table 5.3 and Table 5.4. After completing slotting operations with recommended cutting parameters, average feed and tangential force values are entered to code as upper boundaries for force calculations. Predicted force components in feed and tangential direction is verified with the test results. It is concluded that the code calculations are reliable as it can be seen in Figure 5.17 and Figure 5.18. Figure 5.19 shows that the forces are kept at maximum values during operations with optimized values. After completing the first set of tests, average force values for feed force and tangential force are entered in the code as the upper bounds of the relevant forces. Calculated forces remained under the average force values from the experiments with recommended cutting parameters. Average force in feed direction is reduced by 7.7% and in tangential direction by 16.4% which is shown in Figure 5.19.

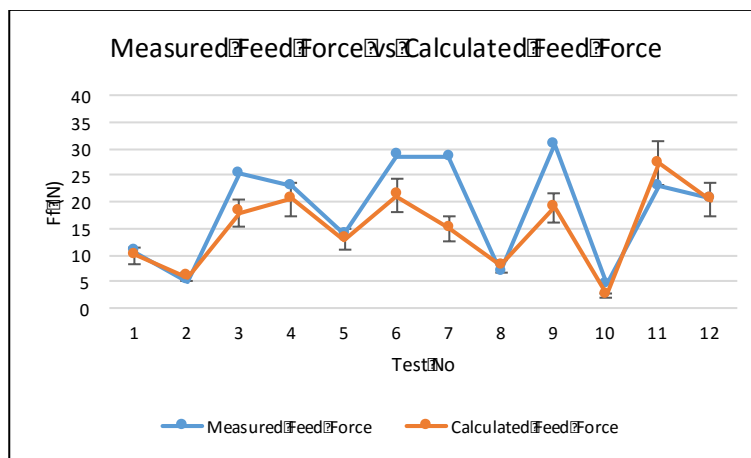


Figure 5.17 - Measured Feed Force vs Calculated Feed Force

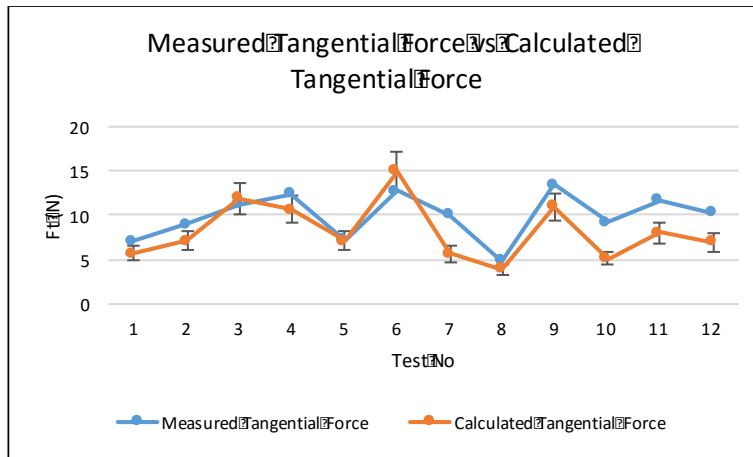


Figure 5.18 - Measured Tangential Force vs Calculated Tangential Force

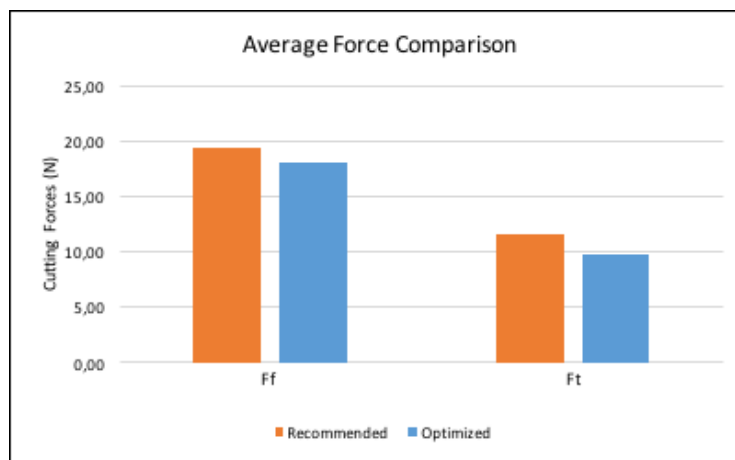


Figure 5.19 – Cutting forces with recommended cutting parameters vs optimized cutting parameters

5.2.5 Summary

In micromilling operations, demand for high surface quality and geometrical accuracy increases production costs. On the other hand, high cutting forces cause short tool life and limits material removal rate, as well as the production time. Optimizing cutting parameters in order to find a balance between production time and cost with high part quality and production performance has been a target research topic in micromilling for researchers. Methods for solving multiple objective problems have different usages in engineering areas. In this thesis, Multi Objective Particle Swarm Optimization is adapted to optimization of micromilling in order to solve for cutting parameters for high part quality and better process performances. This method is selected for its easy adaptation and high computational efficiency. A MATLAB code is developed outputting number

of roughing passes and depth of cut for each roughing pass and finishing pass, cutting velocity and feed for each pass. Pareto curve representing the relation between the production time and production cost is drawn. Surface roughness, burr size and cutting forces are kept under given values.

For verification, a set of experiments are designed. Calculations for production cost, production time, surface roughness and cutting forces are verified by applying tests with the output values for cutting parameters. The results are also compared with the results of another set of tests which are done with the average standard cutting parameters used in literature or recommended by the tool manufacturer. It is observed that both production time and the production cost is lowered. Surface roughness, burr size and cutting forces are kept under control successfully. Predicted results, experimental results and their comparison are presented in this section.

6. CONCLUSION

As mentioned earlier in Chapter 5, optimization of micromilling process is provided using multi objective particle swarm optimization (MOPSO) method. The code predicted values for production time, production cost, surface roughness, burr size and cutting forces. These predicted values are compared with experimental values. It can be concluded that the predicted values are reliable. Another comparison has been made with results obtained from tests with recommended cutting parameters. Following results are achieved:

Production time is calculated during tests with optimized parameters and recommended parameters. It is observed that the production time is reduced by %40 from the first set of tests to second one.

Reduction of production cost is depicted by the change in tool wear rate. Since other factors effecting production cost are constants such as labour cost, tool life is kept at maximum level to reduce production cost. After measuring tool wear rate after each test, it is calculated that the tool wear rate is reduced by 21,8%. It is also observed that the higher cutting velocities lead to higher tool wear rates. The reason is that increasing cutting velocity increases the material removal rate, therefore chip load increases on the tool and tool wears more rapidly. Measurement of cutting forces also supports that the tool wear increases with the increasing cutting velocity.

Surface roughness is measured under microscope after each set of tests. It can be concluded that the surface roughness is decreased by %27,5 with the optimization of process parameters. It is observed that when tool wear increases surface roughness also increase since large hone radii causes high surface roughness. It can be also stated that the low feeds cause high surface roughness due to increasing ploughing mechanism.

Burr sizes are observed under microscope and it is clearly seen that with optimized cutting parameters, burr sizes are reduced considerably. At high cutting velocities, burr size gets smaller because of the decreasing effect of ploughing mechanism. As depth of cut increases, burr size increases as well.

Cutting forces are kept at maximum possible force values in order to provide maximum material removal rates and minimum production time. Cutting force values show increasing trendline as tool wear increases. Force in feed direction is reduced by 7.7% and in tangential direction by 16.4%.

The algorithm developed successfully solves optimization of micromilling process. It is now possible to use process parameters given by the code which would provide better productivity and part quality. It can be concluded that particle swarm optimization can be used as a solution method for multiple objective optimization of micromilling process to improve part quality and process performance. As a suggestion for further researches, other multiple objective optimization methods can be used for micromilling operations in order to reveal best applicable method for micromilling.

There are several MOPSO parameters used in the algorithm such as number of particles, dimension, maximum change a particle can take, learning factors and inertia weight, and also some constants relevant to neighbourhood topology and mutation operator. There are common usages of certain values for these parameters in the literature, however for future work, fine-tuning of these parameters for micromilling operations can be developed.

There are three process parameters calculated by the presented algorithm. An extensive algorithm can be developed which also optimizes other cutting parameters or tool parameters for better tool selection for a specific type of operation.

Since the path length is manually entered to the algorithm, it is hard to implement the code for complex part geometries. The algorithm can be developed and merged with CAM file to calculate path length to provide optimization results specific to part geometry. It can also be merged with a path scheduling algorithm in order to provide a better reduction in production time.

7. REFERENCES

- [1] A. Aramcharoen, P. Mativenga, S. Yang, K. Cooke and D. Teer, "Evaluation and Selection of Hard Coatings for Micromilling of Hardened Tool Steel," *International Journal of Machine Tools and Manufacture*, vol. 48, no. 14, pp. 402-407, 2008.
- [2] U. Natarajan, P. Periyanan and S. H. Yang, "Multiple-response Optimization for Micro-endmilling Process Using Response Surface Methodology," *International Journal of Advanced Manufacturing Technology*, vol. 56, pp. 177-185, 2011.
- [3] H. Bakioglu, "Modeling of Cutting Forces for Precision Milling," Istanbul, 2015.
- [4] C. Celebi, E. Ozlu and E. Budak, "Modeling and Experimental Investigation of Edge Hone and Flank Contact Effects in Metal Cutting," *14th CIRP Conference on Modeling of Machining Operations*, vol. 8, pp. 194-199, 2013.
- [5] R. Lekkela, V. Bajpai, R. Singh and S. Joshi, "Characterization and Modeling of Burr Formation in Micro-end Milling," *Precision Engineering*, vol. 35, pp. 627-637, 2011.
- [6] M. Annoni, S. Petro, Q. Semeraro and R. Solito, "Process Parameters Effect on Cutting Forces and Geometrical Quality in Thin Wall Micromilling," in *Proceeding of NAMRI/SME 41*, 2013.
- [7] H. Sooraj and J. Mathew, "Multi Objective Optimization of Cutting Parameters in Micro-milling of Ti-6Al-4V Alloy," in *All India Manufacturing Technology, Design and Research Conference*, Guwahati, 2014.
- [8] M. Rahman, A. Senthil and J. Prakash, "Micro Milling of Pure Copper," *Journal of Materials Processing Technology*, vol. 116, no. 1, pp. 39-43.
- [9] I. N. a. Tansel, T. a. Arkan, W. Y. a. Bao, N. a. Mahendrakar, B. b. Shisler, D. b. Smith and M. b. McCool, "Tool Wear Estimation in Micro-Machining. Part I: Tool Usage-Cutting Force Relationship," *International Journal of Machine Tools & Manufacture*, vol. 40, pp. 599-608, 2000.
- [10] B. Martin, J. Morrow, P. Heaney and F. Pfefferkorn, "Observation of Tool Life of Micro End Mills," in *Proceedings of the 8th International Conference on MicroManufacturing*, Victoria, Canada, 2013.

- [11] F. W. Taylor, *On the Art of Cutting Metals*, New York: American Society of Mechanical Engineers, 1906.
- [12] S. M. Wu, "Tool Life Testing by Response Surface Methodology," *Journal of Engineering for Industry*, p. 105, 1964.
- [13] E. Kuljanic and V. Solaja, "Random Strategy Method for Determining Tool Life Equations," *CIRP Annals - Manufacturing Technology*, vol. 29, pp. 351-356, 1980.
- [14] S. Kajaria, "Modeling of Tool Life and Micro-mist Flow for Effective Micro-machining of 316L Stainless Steel," 2009.
- [15] K. Liu, *Process Modeling of Micro-Cutting Including Strain Gradient Effects*, Georgia Institute of Technology, 2005.
- [16] R. A. Guimaraes, A. Barcelo, T. Wagner and A. Georgiadis, "Tool Wear Monitoring and Prediction in Micro Milling Process for Medical Applications. Experimental Analysis and Characterization of Tool Wear for Titanium Materials," *Sustainable Design and Manufacturing*, vol. 14, pp. 606-617, 2014.
- [17] P. Twardowski, S. Legutko, G. M. Krolczyk and S. Hloch, "Investigation of Wear and Tool Life of Coated Carbide and Cubic Boron Nitride Cutting Tools in High Speed Milling," *Advances in Mechanical Engineering*, vol. 7, no. 6, pp. 1-9, 2015.
- [18] P. Periyanan, U. Natarajan and S. Yang, "A Study on the Machining Parameters Optimization of Micro-end Milling Process," *International Journal of Engineering, Science and Technology*, vol. 3, no. 6, pp. 237-246, 2011.
- [19] S. Merdol and Y. Altintas, "Virtual Cutting and Optimization of Three-Axis Milling Process," *International Journal of Machine Tools and Manufacture*, vol. 48, pp. 1063-1071, 2008.
- [20] M. Malekian, M. Mostofaa and S. Park, "Modelling of Minimum Uncut Chip Thickness in Micro Machining of Aluminum," *Journal of Materials Processing Technology*, vol. 212, no. 3, pp. 553-559, 2012.
- [21] J. Chae, S. Park and T. Freiheit, "Investigation of Micro-cutting Operations," *International Journal of Machine Tools & Manufacture*, vol. 46, pp. 313-332, 2006.

- [22] K. Yang, Y. Liang, K. Zheng, Q. Bai and W. Chen, "Tool Edge Radius Effect on Cutting Temperature in Micro-end-milling Process," *International Journal of Advanced Manufacturing Technology*, vol. 52, pp. 905-912, 2011.
- [23] M. Vogler, R. Vogler, S. DeVor and Kapoor, "On the Modeling and Analysis of Machining Performance in Micro-endmilling, Part I: Surface Generation," *Journal of Manufacturing Science and Engineering*, vol. 126, no. 4, pp. 685-694, 2004.
- [24] L. Hongtao, "Modelling and Experimental Analysis of the Effects of Tool Wear, Minimum Chip Thickness and Micro Tool Geometry on the Surface Roughness in Micro-end-milling".
- [25] Z. J. Yuan, M. Zhou and S. Dong, "Effect of Diamond Tool Sharpness on Minimum Cutting Thickness and Cutting Surface Integrity in Ultraprecision Machining," *J. Mater. Process. Technol*, vol. 62, pp. 327-330, 1996.
- [26] L. Chengfeng, L. Xinmin, L. Hongtao and N. Jun, "Modeling of Three-dimensional Cutting Forces in Micro-end-milling," *Publishing Journal of Micromechanics and Micro Engineering J. Micromech. Microeng.*, vol. 17, pp. 671-678, 2007.
- [27] E. Hatipoglu , "Experimental Investigation of Surface Formation and Tool Wear in Micromilling," Istanbul, 2015.
- [28] S. Ko and D. Dornfeld, "A Study on Burr Formation Mechanism," *Journal of Engineering and Materials and Technology*, vol. 113, no. 1, pp. 75-87, 1991.
- [29] Z. Kou, Y. Wan, Y. Cai, X. Liang and Z. Liu, "Burr Controlling in Micro Milling with Supporting Material Method," in *43rd Proceedings of the North American Mnaufacturing Research Institution of SME*, 2015.
- [30] C. Chu and D. Dornfeld, "Tool Path Planning for Avoiding Exit Burr," *Journal of Manufacturing Process*, vol. 2, no. 2, pp. 116-123, 2000.
- [31] L. Gillespie and P. Blotter, "The Formation and Properties of Machining Burr," *ASME J Engineering Industry*, vol. 98, no. 1, pp. 66-74, 1976.
- [32] T. Komatsu, Yoshino T., T. Matsumura and S. Torizuka, "Effect of Crystal Grain Size in Stainless Steel on Cutting Processes in Micromilling," in *Procedia CIRP 1.0*, 2012.

- [33] K. Saptaji , S. Subbiah and J. Dhupia, “Effect on Side Edge Angle and Effective Rake Angle on Top Burrs in Micro-Milling,” *Precision Engineering*, vol. 36, no. 3, pp. 444-450, 2012.
- [34] E. Kuram and B. Ozcelik, “Multi-Objective Optimization using Taguchi Based Grey Relational Analysis for Micro-Milling of Al 7075 Material with Ball Nose End Mill,” *Measurement*, vol. 46, no. 6, pp. 1849-1864, 2013.
- [35] M. Chen, H. Ni, Z. Wang and Y. Jiang, “Research on the Burr Modeling of Burr Formation Process in Micro-Ball End Milling Operation on Ti-6Al-4V,” *The International Journal of Advanced Manufacturing Technology*, vol. 62, pp. 901-912, 2012.
- [36] G. Schueler, J. Engmann, T. Marx, R. Haberland and J. Aurich, “Burr Formation and Surface Characteristics in Micro-end Milling of Titanium Alloys,” *Burrs-Analysis, Control and Removal*, pp. 129-138, 2010.
- [37] K. Weinert and V. Petzoldt, “Machining NiTi Micro-parts by Micro-milling,” *Materials Science and Engineering*, pp. 672-675, 2008.
- [38] P. Cardoso and J. P. Davim, “Micro Milling of Metallic Materials - A Brief Overview,” *Transactions of Famena*, vol. 36, no. 2, pp. 79-85, 2012.
- [39] J.-D. Kim and D. Kim, “Theoretical Analysis of Micro-cutting Characteristics in Ultra Precision Machining,” *J Mater Process Technol*, vol. 49, pp. 387-398, 1995.
- [40] G. Bissacco, H. Hansen and J. Slunsky, “Modelling the Cutting Edge Radius Size Effect for Force Prediction in Micro Milling,” *CIRP Annals - Manufacturing Technology*, vol. 57, pp. 113-116, 2008.
- [41] X. Jin and Y. Altintas, “Slip-line Field Model of Micro-Cutting Process with Round Tool Edge Effect,” *Journal of Materials and Physics of Solids*, vol. 211, pp. 339-355, 2011.
- [42] N. Fang, “Line Modelling of Machining with a Rounded Edge Tool, Part I: New Model and Theory,” *Journal of Mechanics and Physics of Solids*, vol. 51, pp. 715-742, 2003.
- [43] Y. Altintas and X. Jin, “Mechanics of Micro-Milling with Round Edge Tools,” *CIRP Annals - Manufacturing Technology*, vol. 60, pp. 77-80, 2011.
- [44] M. Malekian, S. Park and M. Jun, “Modeling of Dynamics Micro-Milling Cutting Forces,” *International Journal of Machine Tools and Manufacture*, vol. 49, pp. 586-598, 2009.

- [45] S. Park and M. Malekian, "Mechanistic Modeling and Accurate Measurement of Micro End Milling Forces," *CIRP Annals - Manufacturing Technology*, vol. 58, pp. 49-52, 2009.
- [46] W. Y. Bao and I. N. Tansel, "Modeling Micro-End Milling Operations. Part I: Analytical Cutting Force Model, *International Journal of Machine Tools and Manufacture*," vol. 49, pp. 2155-2173, 2000.
- [47] S. M. Afazov, S. M. Ratchev and J. Segal, "Modeling and Simulation of Micro-Milling Cutting Forces," *Journal of Materials Processing Technology*, vol. 126, pp. 2154-2162, 2010.
- [48] E. Budak, E. Ozlu, H. Bakioglu and Z. Barzegar, "Thermo-mechanical Modeling of the Third Deformation Zones in Machining for Prediction of Cutting Forces," *CIRP Annals - Manufacturing Technology*, vol. 65, no. 1, pp. 121-124, 2016.
- [49] T. H. Childs , K. Maekawa, T. Obikawa and Y. Yamane, *Metal Machining: Theory and Applications*, London, 2000.
- [50] T. Wu, "Tooling Performance in Micro Milling Modelling, Simulation and Experimental Study," Brunel University, 2012.
- [51] P. Li, "Micromilling of Hardened Tool Steels," Delft University of Technology, 2009.
- [52] F. Fang, H. Wu, X. Liu, Y. Liu and S. Ng, "Tool Geometry Study in Micromachining," *Journal of Micromechanics and Microengineering*, vol. 13, pp. 726-731, 2003.
- [53] W. Y. Bao and I. N. Tansel, "Modeling Micro End Milling Operations. Part II: Tool Run-out," *International Journal of Machine Tools & Manufacture*, vol. 40, pp. 2175-2192, 2000.
- [54] J. Aurich, I. Reichenbach and G. Schüler, "Manufacture and application of ultra-small micro end mills," *CIRP Annals - Manufacturing Technology*, vol. 61, no. 1, pp. 83-86, 2012.
- [55] C. Torres, P. Heaney, A. Sumant, M. Hamilton, R. Carpick and F. Pfefferkorn, "Analyzing the Performance of Diamond-Coated Micro End Mills," *International Journal of Maching Tools and Manufacture*, vol. 49, no. 7-8, pp. 599-612, 2009.
- [56] E. Uhlmann and K. Schauer, "Dynamic Load and Strain Analysis for the Optimization of Micro End Mills," *CIRP Annals - Manufacturing Technology*, vol. 54, no. 1, pp. 75-78, 2005.

- [57] X. Cheng, Z. Wang, K. Nakamoto and K. Yamazaki, "Design and Development of PCD Micro Straight Edge End Mills for Micro/Nano Machining of Hard and Brittle Materials," *Journal of Mechanical Science and Technology*, vol. 24, no. 11, pp. 2261-2268, 2010.
- [58] P. Depince and J. Y. Hascoet, "Active Integration of Tool Deflection Effects in End Milling. Part 2. Compensation of Tool Deflection," *International Journal of Machine Tools and Manufacture*, vol. 46, pp. 945-956, 2006.
- [59] Z. N. and F. M., "Prediction of Tool Deflection and Tool Path Compensation in Ball-end Milling," *Journal of Intelligent Manufacturing*, vol. 26, pp. 425-445, 2015.
- [60] A. Mamedov, "Mechanics and Thermal Modeling of Micro Milling," Koc University, Istanbul, 2015.
- [61] A. Larue and A. Y., "Simulation of Flank Milling Processes," *International Journal of Machine Tools and Manufacture*, vol. 45, pp. 549-559, 2005.
- [62] S. H. Ryu, H. S. Lee and C. N. Chu, "The Form Error Prediction in Side Wall Machining Considering Tool Deflection," *International Journal of Machine Tools and Manufacture*, vol. 43, pp. 1405-1411, 2003.
- [63] G. M. Kim, B. H. Kim and C. N. Chu, "Estimation of Cutter Deflection and Form Error in Ball-end Milling Processes," *International Journal of Machine Tools and Manufacture*, vol. 43, pp. 917-924, 2003.
- [64] V. S. Rao and R. P. V., "Tool Deflection Compensation in Peripheral Milling of Curved Geometries," *International Journal of Machine Tools and Manufacture*, vol. 46, pp. 2036-2043, 2006.
- [65] P. Rodriguez and J. E. Labarga, "Tool Deflection Model for Micromilling Processes," *The International Journal of Advanced Manufacturing Technology*, vol. 76, pp. 199-207, 2014.
- [66] J. Li, X. Yang, C. Ren, G. Chen and Y. Wang, "Multiobjective Optimization of Cutting Parameters in Ti-6Al-4V Milling Process Using Nondominated Sorting Genetic Algorithm - II," *International Journal of Advanced Manufacturing Technology*, vol. 76, pp. 941-953, 2015.

- [67] T. Thepsonthi and T. Ozel, "Multi-objective Process Optimization for Micro-end Milling of Ti-6Al-4V Titanium Alloy," *International Journal of Advanced Manufacturing Technology*, vol. 63, pp. 903-914, 2012.
- [68] T. Thepsonthi, *Modeling and Optimization of Micro-Eng Milling Process for Micro-Manufacturing*, New Brunswick, New Jersey, 2014.
- [69] Z. Shi, Z. Liu, Y. Li and Y. Qiao, "Swept Mechanism of Micro-Milling Tool Geometry Effect on Machined Oxygen Free High Conductivity Copper (OFHC) Surface Roughness," *Materials*, vol. 10, 2017.
- [70] A. Yusoff, S. Turner and C. Taylor, "The Role of the Tool Geometry in Process Damped Milling," *International Journal of Advanced Manufacturing Technology*, vol. 50, pp. 883-895, 2010.
- [71] K. S. S. Saptaji, "Effect of Side Edge Angle and Effective Rake Angle on Top Burrs in Micro-Milling," *Precision Engineering*, vol. 36, no. 3, pp. 444-450, 2012.
- [72] V. Pareto, *Manuale di Economia Politica*, Milano: Societa Editrice Libreria, 1906.
- [73] D. K., *Multi-Objective Optimization Using Evolutionary Algorithms*, John Wiley & Sons, Ltd., 2001.
- [74] M. Reyes-Sierra and C. Coello Coello, "Multi-Objective Particle Swarm Optimizers: A Survey of the State-of-the-Art," *International Journal of Computational Intelligence Research*, vol. 2, no. 3, pp. 287-308, 2006.
- [75] R. T. Marler and J. S. Arora, "Survey of Multiple-Objective Optimization Methods for Engineering," *Struct Multidisc Optim*, vol. 26, pp. 369-395, 2004.
- [76] J. Khazaii, *Advanced Decision Making for HVAC Engineers*, Marietta, GA: Springer, 2016.
- [77] S. Jithin, B. Kuriachen and J. Mathew, "Multi-objective Optimization of Micro ED Milling of Ti-6Al-4V using Generic Algorithm," in *International Conference on PRECISION, MESO, MICRO AND NANO ENGINEERING*, Calicut, 2013.
- [78] W. Yang, Y. Guo and W. Liao, "Multi-objective Optimization of Multi-pass Face Milling Using Particle Swarm Intelligence," *International Journal of Advanced Manufacturing Technology*, vol. 56, pp. 429-443, 2011.

- [79] K. Deb, A. Pratap, S. Agarwal and T. Meyarivan, "A Fast and Elitist Multi-Objective Genetic Algorithm: NSGA-II," *IEEE Trans Evol Comput*, vol. 6, pp. 182-197, 2002.
- [80] N. K. Jha, "A Discrete Data Base Multiple Objective Optimization of Milling Operation Through Geometric Programming," *Trans ASME J Eng Ind*, vol. 112, no. 4, pp. 368-374, 1990.
- [81] Z. G. Wang, M. Rahman, Y. S. Wong and J. Sun, "Optimization of Multi Pass Milling Using Generic Algorithm and Generic Simulated Annealing," *Int J Adv Manuf Technol*, vol. 24, pp. 727-732, 2004.
- [82] K. Deb, "Multi-objective Evolutionary Algorithms: Introducing bias Among Pareto-optimal Solutions," KanGAL Report, India, 1999.
- [83] J. Kennedy and R. Eberhart, "Particle Swarm Optimization," in *Proceeding of IEEE International Conference on Neural Networks*, 1995.
- [84] X. Liu, R. DeVor and S. Kapoor, "The Mechanics of Machining at the Microscale: Assessment of the Current State of Science," *Journal of Manufacturing Science and Engineering*, vol. 126, no. 4, pp. 666-678, 2004.
- [85] T. Ozel, X. Lui and A. Dhanorker, "Modelling and Simulation of Micro-milling Process," in *Proceedings of the Fourth International Conference and Exhibition on Design and Production of Machines and Dies/Molds*, Cesme, Turkey, 2007.
- [86] A. Aramcharoen, P. Mativenga, S. Yang, K. Cooke and D. Teer, "Evaluation and Selection of Hard Coatings for Micro Milling of Hardened Tool Steel," *International Journal of Machine Tools and Manufacture*, vol. 48, pp. 1578-1584, 2008.
- [87] X. Liu, R. Devor, S. Kapoor and K. Ehmann, "The Mechanics of Machining at the Microscale; Assesment of the Current State of the Science," *Trans ASME J Manuf Sci Eng*, vol. 126, pp. 666-678, 2004.
- [88] S. Shimada, N. Ikawa, H. Tanaka, G. Ohmuri, J. Uchikoshi and H. Yoshinaga, "Feasibility Study on Ultimate Accuracy in Microcutting Using Molecular Dynamics Simulation," *CIRO Ann.*, vol. 42, pp. 91-94, 1993.
- [89] J. Kennedy and R. Eberhart, "Particle Swarm Optimization," in *Proceedings of the IEEE International Conference on Neural Networks 4*, 1995.

- [90] V. Kachitvichyanukul, "Comparison of Three Evolutionary Algorithms; GA, PSO and DE," *Industrial Engineering & Management Systems*, vol. 11, no. 3, pp. 215-223, 2012.
- [91] E. Vazquez, C. Joaquim, C. Rodriguez, T. Thepsonthi and T. Ozel, "Swarm Intelligent Selection and Optimization of Machining System Parameters for Microchannel Fabrication in Medical Devices," *Materials and Manufacturing Processes*, vol. 26, no. 3, pp. 403-414, 2011.
- [92] G. T. M. S. Carlos A. Coello Coello, "Handling Multiple Objectives with Particle Swarm Optimization," *IEEE Transactions on Evolutionary Computation*, vol. 8, no. 3, pp. 256-279, 2004.
- [93] V. K. a. S. Minz, "Multi-Objective Particle Swarm Optimization: An Introduction," *Smart Computing Review*, vol. 4, no. 5, pp. 335-353, 2014.
- [94] S. S. R. Kalpakjian S, *Manufacturing Engineering and Technology*, NJ: Prentice Hall, Upper Saddle River, 2000.
- [95] P. Kumar, V. Bajpai and R. Singh, "Burr Height Prediction of Ti6Al4V in High Speed Micro-milling by Mathematical Modelling," *Manufacturing Letters*, vol. 11, pp. 12-16, November 2017.
- [96] Y. H. Kang and C. M. Zheng, "Mathematical Modeling of Chip Thickness in Micro-end Milling; a Fourier Modeling.," *Appl. Math Model*, vol. 37, pp. 4208-4223, 2013.
- [97] Y. Altintas, "Metal Cutting Mechanics, Machine Tool Vibrations and CNC Design," in *Manufacturing Automation*, Cambridge University Press, 2000.
- [98] E. Ozlu and E. Budak, "Thermomechanical Modeling of Orthogonal Cutting Including the Effect of Stick - Slide Regions on the Rake Face," *10th CIRP International Workshop on Modeling of Machining Operations*, August 2007.
- [99] N. H. Cook, "Tool Wear and Tool Life," *Journal of Manufacturing Science and Engineering*, vol. 95, no. 4, pp. 931-938, 1973.
- [100] S. Kumar, T. T. M. Kannan, S. Giridharan and V. Kumar, "Optimization of Micro-Milling Parameters of Al-6082 by Anova Methodology," *International Journal of Mechanical Engineering and Robotics Research*, vol. 3, no. 4, 2014.

- [101] A. Yusoff and N. Sims, "Optimization of Variable Helix Tool Geometry for Regenerative Chatter Mitigation," *International Journal of Machine Tools & Manufacture*, vol. 51, pp. 133-141, 2011.
- [102] C. Pornsing, M. Sodhi and B. Lamond, "Novel Self-adaptive Particle Swarm Optimization Methods," *Soft Comput*, vol. 20, pp. 3579-3593, 2016.